

Heterogeneous ice nucleation on mineral dust particles

DIPLOMARBEIT

zur Erlangung des akademischen Grades

Diplom-Ingenieur

im Rahmen des Studiums

Materialchemie

eingereicht von

Tobias Zolles

Matrikelnummer 0726402

an der

Fakultät für Technische Chemie der Technischen Universität Wien

Betreuung: Ao.Univ.Prof. Dipl.-Chem. Dr.rer.nat. Hinrich Grothe

Wien, 20.08.2013

(Unterschrift Tobias Zolles)

(Unterschrift Betreuung)



Heterogeneous ice nucleation on mineral dust particles

MASTER'S THESIS

submitted in partial fulfillment of the requirements for the degree of

Master of science

in

Materials chemistry

by

Tobias Zolles

Registration Number 0726402

to the Faculty of Technical Chemistry
at the Vienna University of Technology

Advisor: Ao.Univ.Prof. Dipl.-Chem. Dr.rer.nat. Hinrich Grothe

Vienna, 20.08.2013

(Signature of Author)

(Signature of Advisor)

Erklärung zur Verfassung der Arbeit

Tobias Zolles
Feldgasse 26, 2511 Pfaffstätten

Hiermit erkläre ich, dass ich diese Arbeit selbständig verfasst habe, dass ich die verwendeten Quellen und Hilfsmittel vollständig angegeben habe und dass ich die Stellen der Arbeit - einschließlich Tabellen, Karten und Abbildungen -, die anderen Werken oder dem Internet im Wortlaut oder dem Sinn nach entnommen sind, auf jeden Fall unter Angabe der Quelle als Entlehnung kenntlich gemacht habe.

(Wien, 20.08.2013)

(Unterschrift Tobias Zolles)

Danksagung

Es war nicht immer leicht sich für alle Messungen und Recherchen für diese Masterarbeit zu begeistern. Ich danke vorallem den Personen, die mich mental unterstützt haben und mir neue Kraft gegeben haben, insbesondere meinen Eltern Karl und Irene Zolles, meiner Schwester Isabella Zolles und allen Tourenpartner auf den Bergtouren aus denen ich so viel Kraft geschöpft habe.

Weiters möchte ich mich bei Werner Artner, Klaudia Hradil und dem Röntgenzentrum der TU Wien die mir mit den XRD Messungen, XRD Analysen und einige Diskussionen geholfen haben, bedanken. Karin Whitmore und Johannes Bernardi vom USTEM der TU Wien gilt Dank für die durchgeführten elektronenmikroskopischen Messungen.

Ich möchte mich bei meinem Betreuer Ao.Prof. Hinrich Grothe für die Möglichkeit diese Arbeit durchführen zu dürfen bedanken, sowie den zahlreichen positiven Diskussionen und Gesprächen und der Assistenz. Bernhard Pummer danke ich für die Einführung in die Kryo-Mikroskopie und Johannes Frank für das Mikroskop.

Zu guter Letzt möchte ich dem FWF für die finanzielle Unterstützung meiner Masterarbeit danken.

Abstract

Ice nucleation activities of mineral dust particles were investigated. The experiments were carried out using cryo-microscopy which is an oil-emulsion based method. The immersion freezing mode was addressed with this experimental setup. The studied samples were common inorganic atmospheric aerosols. Single minerals and natural samples were tested. Mineral dust particles are active ice nuclei in the immersion freezing mode up to $256K/ -17^{\circ}C$. The nucleation temperatures of mineral dusts are much lower than for biological ice nuclei. K-feldspar is the by far most active ice nuclei followed by other silicates. Natural samples which contain more than 5% K-feldspar were also active. The activity of K-feldspar can be attributed to its surface structure and the presence of potassium ions in the surface.

Ice nucleation on mineral dust particles takes place at certain nucleation sites. These sites are domains of molecular sites where water is stabilized in an ice-like structure. To form a good ice nucleation site, the site density of molecular sites needs to be high. More molecular sites are able to form larger domains on the surface, leading to better nucleation sites. This suggests further that the nucleation temperature of mineral dust particles scales with the surface area. The exact configuration of a molecular site is material specific and influenced by the local chemistry and structure of the dust particle surface. A favorable arrangement of the functional groups like surface hydroxyl and oxygen is proposed for the K-feldspar. Potassium ions seem to have a positive or neutral effect on the ice nucleation property of a silicate surface while cations with a higher charge density like calcium and sodium have a negative influence. K-feldspar is abundant in the environment and actually is the most important dust ice nucleus in the atmosphere. The nucleation temperatures of the K-feldspar particles are sufficient to enable further meteorological glaciation processes in high altitude clouds.

Kurzfassung

In Rahmen dieser Arbeit wurden die Eisnukleationsaktivitäten von Mineralstaubpartikeln untersucht. Die Experimente wurden mit Hilfe eines Kryo-Mikroskops und der Öl-Emulsions-Technik, durchgeführt. Mit dieser Methode ist es möglich das Immersionsgefrieren von Wassertropfen zu untersuchen. Bei den untersuchten Proben handelt es sich um anorganische atmosphärische Aerosolpartikel. Es wurden sowohl einzelne Mineralien als auch natürliche Staubproben untersucht. Mineralstaubpartikel sind aktive Eiskeime im Immersionsmodus bis zu Temperaturen von $256K / -17^{\circ}C$. Damit sind Mineralstäube bei geringeren Temperaturen aktiv als einige biologische Substanzen. Kaliumfeldspat ist der aktivste Mineralstaub, der untersucht wurde, auch andere Silikatminerale waren aktive Eiskeime. Alle Naturproben, die Kaliumfeldspat enthalten, waren auch aktiv, falls der Feldspatgehalt mindesten 5% betrug. Die Aktivität von Kaliumfeldspat ist eine Folge seiner Oberflächenstruktur und den dort vorhandenen Kaliumionen.

Die Eisnukleation an Mineralstaubpartikeln findet an lokalen Nukleationsstellen auf der Oberfläche der Partikel statt, wo die Keimbildung ausgelöst wird. Diese lokalen Stellen sind Domänen von molekularen Gruppen, wo Wassermoleküle in einer eis-ähnlichen Struktur stabilisiert werden. Gute Nukleationsstellen sind auf Partikeln mit einer größeren Dichte an molekularen Gruppen zu finden. Daraus folgt, dass sich die Nukleationstemperatur durch Vergrößerung der Partikeloberfläche teilweise erhöht. Die genaue Struktur einer molekularen Gruppe ist materialspezifisch und hängt von der lokalen chemischen Konfiguration und Struktur der Partikeloberfläche ab. In Kaliumfeldspat gibt es entsprechend günstige Konfigurationen von Hydroxy- and Oxy-gruppen. Die Kaliumionen scheinen einen positiven oder zumindest neutralen Effekt auf die Eisnukleation von Silikaten zu haben, im Gegensatz zu Ionen mit höherer Ladungsdichte wie Kalzium oder Natrium. Der Kaliumfeldspat ist reichlich in der Umwelt vorhanden und entsprechend der wichtigste mineralische Eiskeim. Die Keimbildungstemperaturen von Kaliumfeldspatpartikeln sind hoch genug um weitere meteorologische Eisbildungsprozesse in großer Höhe in Wolken zu ermöglichen.

Contents

1	Introduction	1
1.1	The atmosphere	1
1.2	Water phases	6
1.3	Atmospheric aerosols	11
2	Experimental	15
2.1	Sample selection	15
2.2	Methods	17
2.3	Sample preparation	25
3	State of the art	27
4	Results	33
4.1	Non silicate materials	34
4.2	Silicate materials	37
5	Discussion	53
5.1	Ice nucleation of the different dust particles	55
5.2	Comparison between ice nucleation on different samples and materials . .	68
5.3	Atmospheric impacts of mineral dust particles	69
6	Conclusion and outlook	71
	List of used characters	73
	List of Figures	74
	List of Tables	75
	Bibliography	77

Introduction

1.1 The atmosphere

The atmosphere is a mantle of gases surrounding the Earth, which is divided into five main layers based on the temperature gradient. The atmosphere plays a major role on the climate of the Earth. Life would not be possible without it on the planet. The atmosphere influences the temperature and radiation balance of the Earth. Gases in the atmosphere absorb incoming and outgoing radiation. The earth atmosphere consists mainly of nitrogen, oxygen and argon. The local variability of these components is quite low. Trace gases are carbon dioxide, carbon monoxide, hydrogen, methane, nitrogen oxides, ozone, the noble gases neon, xenon, helium and water. The concentration of these gases has a high regional and seasonal variability. Water can also be present as liquid or solid, and is in this section not considered as a main component or a trace gas. The mean concentrations are given in table 1.1.

Table 1.1: The atmospheric gas composition

Atmospheric gas composition				
Main Components			Important trace gases	
78%	N_2		390+ppm	CO_2
21%	O_2		<2ppm	CH_4
0,9%	Ar		<500ppb	N_2O
			550ppb	H_2

The atmosphere is no clean gas environment, but many aerosols are present. Water is the most important tropospheric aerosol for the earth climate. It has a large influence on the radiation balance, but the exact quantity is unknown. Aqueous aerosols have a large impact on the local weather and global climate. The earth atmosphere consists of five main layers: The troposphere extends from the surface of the Earth up to a

height of 10-15km. In this layer all the weather phenomena and the water cycle take place. Most clouds form in the troposphere. 99% of the atmospheric water and aerosol particles are found in the troposphere. The temperature is decreasing with height within this atmospheric layer. The next layer is the stratosphere, which reaches up to 50km. The temperature increases with height in that layer due to the UV absorption of the oxygen species which form a photochemical equilibrium at elevated concentrations. The mesosphere extends from the stratopause up to 80km [42]. In this layer few more aerosols are present due to the burning of meteors. The temperatures in this layer are quite low with around 193K. So-called nocturnal clouds form in this layer. The water present at this altitude is not part of the water cycle. The water is rather formed by chemical reactions of methane. The cold temperatures do favor ice cloud formation. The role of the present aerosols is unknown in this process. The last two layers are the thermosphere and the exosphere. These layers are quite low in density and do not have a high influence on the earth climate. Over the whole atmosphere the pressure is exponentially decaying with altitude.

1.1.1 Clouds

A cloud consists of aerolized liquid or solid particles. Clouds are referred to as a visible ensemble of these aerosols. Water clouds are condensed water molecules in the atmosphere. There exist three principal types of clouds: water clouds, mixed-phase clouds

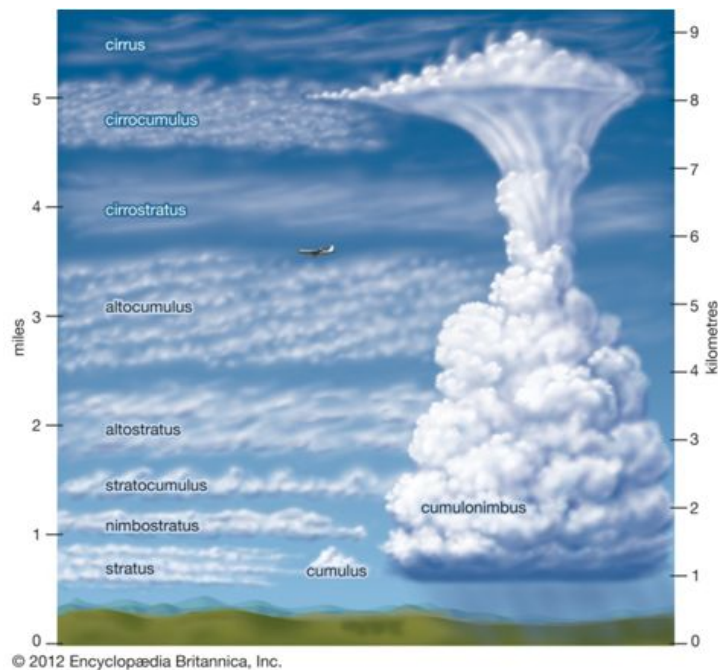


Figure 1.1: The different cloud types in the atmosphere. The displayed cloud heights are only an approximation and may vary in reality depending on the meteorological conditions.

and ice clouds. The first two do only occur in the troposphere, while ice clouds are present up to the mesosphere. Since the early 19th century a cloud classification exists. The principal types of clouds are cirrus, cumulus, cumulonimbus and stratus. The clouds appear in different shape, reflectivity and height. Depending on the meteorological conditions different type of clouds form. In figure 1.1 an overview about the clouds in the troposphere is given. Nevertheless the internal physical conditions in the same cloud type may be quite different. Temperature, liquid water content, pressure and density may vary largely [42].

In general clouds form if the water saturation of air is exceeded. The water saturation does decrease with temperature, therefore colder air masses increase in relative moisture RH . If an air parcel is up drafted the parcel expands adiabatically due to the lower pressure. This expansion cools the air masses and therefore leads to an increased water saturation. If full saturation is reached, the system is not in thermodynamic equilibrium. The water vapor should decrease by drop or ice formation, but it is a kinetically hindered transition at atmospheric conditions. Therefore nuclei are needed. Cloud condensation nuclei (CCN) catalyze water droplet formation and ice nuclei (IN) nucleate solid water/ice particles.

The formed water drops are typically in the low micrometer range [42]. These small drops are the reason for the typical white appearance of clouds, due to forward Mie scattering [2, 42]. The drops are too small to precipitate. Smaller drops have a slightly higher vapor pressure than large ones, resulting in evaporation of the small ones. This is leading to larger drops which are heavy enough to fall down. Nevertheless upon falling these small single drops would evaporate, in fact they collide with further drops and finally form raindrops. Ice nucleation processes lead to ice particles within the cloud. The ice particles grow on cost of water vapor or water drops.

1.1.2 Radiation balance

The earth radiation and heat balance may be split in incoming and outgoing parts. Compared to the sunlight other extraterrestrial heat sources can be neglected. Only around 50% of the solar radiation at exosphere level reaches the ground of the atmosphere. The rest is either reflected back or absorbed by the atmosphere. The atmosphere is a selective absorber. Atmosphere gases absorb at their characteristic wavelength. The highest amount of energy is absorbed in the UV range by oxygen and oxygen species. The resulting average solar spectrum at ground level is given in figure 1.3. Atmospheric aerosols reflect 20-25% of the solar light back into space. Water clouds are the most important aerosols. The reflection performance of the aerosols can be given by the albedo. The albedo of a substance gives its diffuse reflectivity. White objects have generally a higher albedo than dark ones. Clouds contribute to more than 50% of earth reflectivity of solar radiation, but the exact impact of clouds on the radiation balance is unknown. All cloud types have a higher albedo than most of earth surface and therefore have a net cooling effect on the Earth. Ice clouds have an even higher albedo than water clouds. Upon glaciation the albedo of a cloud increases, but its tendency to precipitate increases (see section 1.2.1).

The earth surface reflects less than 15% of the incoming solar radiation. The albedo of the surface varies highly. While glaciated areas reflect up to 90%, the ocean or forested areas are good absorbers.

Heat is also transported upwards by air. Up drifting warmer air parcels remove heat

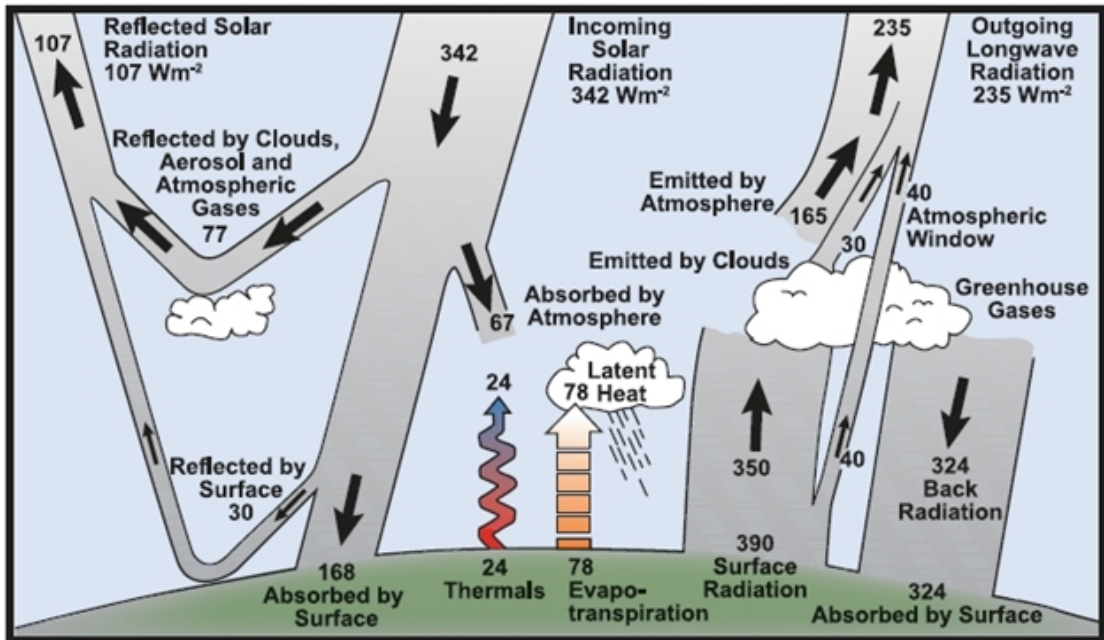


Figure 1.2: Radiation balance of the Earth. Figure taken from Kiehl et al. [21].

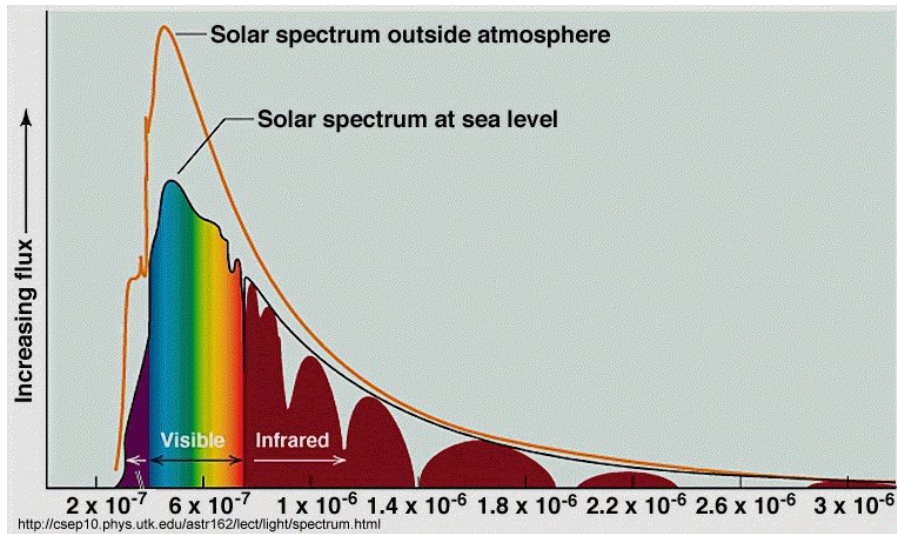


Figure 1.3: The intensity of the light at certain wavelength decreases due to absorption by atmospheric gases and aerosols. The IR-window can be seen here too.

from the lower layers, this is marked with thermals in the figure (1.2). The vaporization of water on the earth surface takes high amounts of heat (see section 1.2). But this heat is released again upon the condensation and ice formation in the atmosphere. The precipitates transfer some of the heat back to Earth surface. The heat of the phase change of water is never lost in this water cycle, but the formed clouds emit long-wave (infrared) radiation depending on their temperature. The heat in this water cycle is called latent heat in figure 1.2.

The Earth emits mainly long-wave (infrared) radiation. The radiation is partly absorbed by the atmosphere. This effect is known as the greenhouse (gas) effect. Molecules like CO_2 , CH_4 or N_2O absorb the long-wave radiation emitted by the Earth. There is only a small spectral region where the radiation is only absorbed a tiny bit. This part of the spectral range is called the atmospheric or infrared window ($350 - 800cm^{-1}$). But the radiation is still absorbed and scattered by clouds. As a result clouds do also have a heating effect or, to be more precise, reduce the cooling of the earth surface. Gases and aerosols of the atmosphere also emit long wave radiation, around one third of which is emitted out to space.

1.2 Water phases

Water is the molecule H_2O . It has an angled structure (C_{2v} -symmetry) with a bonding angle of around $104,5^\circ$ (fig.: 1.4) . The molecule has a high dipolar moment of $6,2 \cdot 10^{-30} Cm$ due to the high difference in electronegativity of the atoms and the angled structure. This high dipolar moment results in huge intermolecular interactions. Hydrogen bonding interactions (strong dipolar interactions) are so strong that the melting point and boiling points are at quite high temperature under terrestrial conditions for such small molecules in comparison to other main group compounds. Water has a large heat capacity of around $4,2 Jg^{-1}K^{-1}$. The heat of vaporization is around $40 kJmol^{-1}$ and enthalpy of fusion (melting) $330 kJkg^{-1}$. The presence of all three phases solid, liquid and gaseous on earth enables the complex water cycle on earth. In figure 1.5 the phase diagram for water is given. Under standard terrestrial conditions ($p=1bar$), water freezes at $273K$ and boils at $373K$. There are other solid phases except the hexagonal ice I_h face in general referred to as simply ice, but these are of no interest under atmospheric conditions. Hexagonal ice is a solid structure of water which is thermodynamically stable below $273K$ in pressure regions between Pa [42] Water crystallizes in a sixfold-symmetric structure under these conditions. The unit cell/structure of the I_h crystal is shown in figure 1.6.

The water molecules are in a hexagonal arrangement, connected via hydrogen bonds. Every water molecule is connected to its four nearest neighbors. The four oxygen atoms of the nearest neighbors form tetrahedrons. These tetrahedrons form the hexagonal lattice. Ice has a D_{6dh}^4 symmetry and belongs to the space group $P6_3/mmc$. The ice structure is a kind of layered structure. The six hexagonally arranged water molecules form a layer of these hexagonal rings. Every second water molecule of the hexagonal rings forms a hydrogen bond to the upper layer. By fast cooling to lower temperatures than $193K$ cubic ice I_c can form, where the anisotropy present in hexagonal ice is lost. Macroscopic ice has a transparent, white or bluish appearance depending on the amount

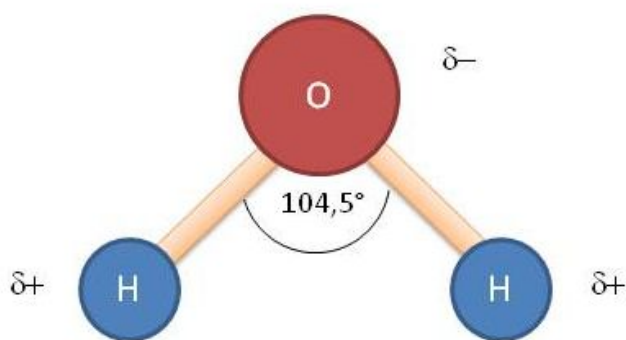


Figure 1.4: The structure of water. The $\delta\pm$ represent polarization charges of the molecule.

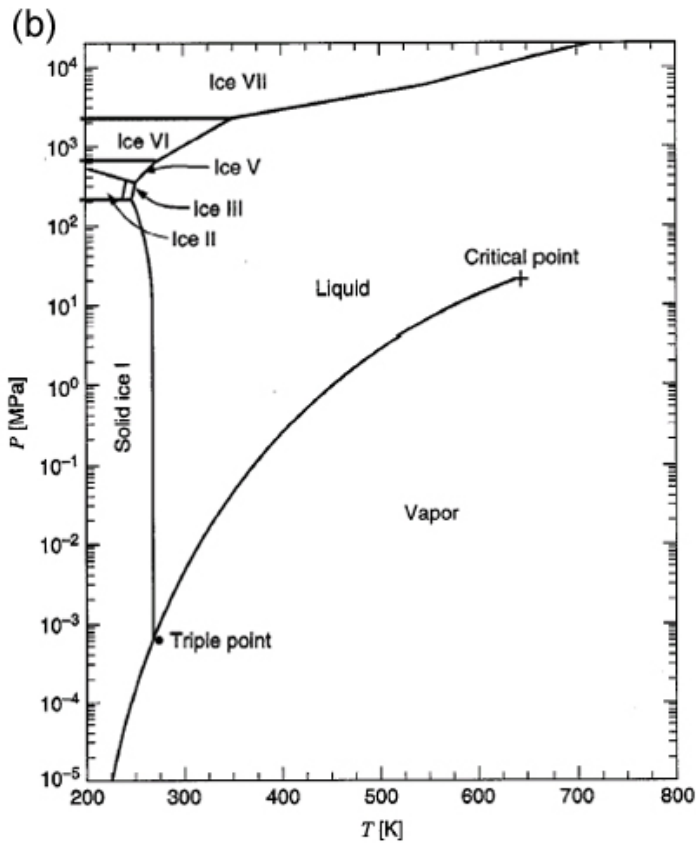


Figure 1.5: Phase diagram for water. Solid ice I represents hexagonal ice, while the other solid phases II-VII are not explained in detail here [5]

of air inside. It is formed in the atmosphere in clouds, riming processes on earth, freezing of sea and freshwater. Ice has a lower density than liquid water.

Liquid water is present in huge quantities on earth. Due to its polarity liquid water has a huge surface tension in respect to air and forms droplets. The density of water first increases with temperature up to 277K . Compared to ice the water molecules come closer in the less rigid structure and the amount of nearest neighbors increases. For higher temperature classical liquid behavior with decreasing density is observed. This density anomaly can be attributed to water molecule clustering.

1.2.1 Cloud processes

„Cloud“ is here always understood as a water cloud. There are three different cloud types: water clouds, mixed phase clouds and ice clouds. The first type consist only of liquid water drops which form the cloud. Fog is a closely related phenomenon on the Earth. These clouds may form from supersaturated air. Small water drops condense either directly, seldom in the troposphere, or on CCN which are present at higher numbers in

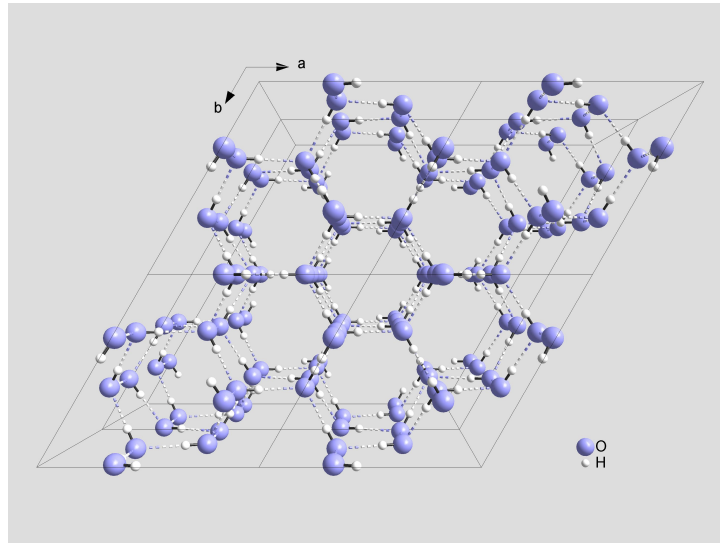


Figure 1.6: The structure of ice I_h showing the oxygen atoms in blue, the hydrogen in white. The image represents a static image of the solid. Bond distances along the OHO bonds vary.

the atmosphere. During condensation the water vapor is removed from the air. The typical water cloud is a cumulus humilis, where warm wet air is rising. The air parcel expands against the lower pressure and therefore cools down. This reduces the water capacity of the air and the relative humidity increases until supersaturation is reached and condensation sets in. In these water clouds several multiplication processes are active.

In mixed phase clouds, ice particles and water drops are present. The formation of ice in these clouds is quite complex. The temperature is not low enough to form ice homogeneously. It is thought that the water drops form first and ice particles are formed later. The ice formation may be formed via different processes explained in the next session. Nevertheless once ice is present in a cloud one can observe different processes depending on the supersaturation with respect to ice and water. If the air is still supersaturated in respect to water, the ice crystals and the water drops will grow. This will finally lead to a point where the air is only supersaturated with respect to ice. Then the so called Bergeron-Findeisen process will set in. The vapor pressure for the water is higher than for ice. As a result the water drops will get smaller and the ice crystals will grow. The ice crystals may collide later and form larger aggregates which may start to precipitate if grown large enough.

Ice clouds consist only of ice crystals. These clouds form at very low temperature i.e. at high altitudes. Typical ice clouds are the cirrus clouds. Their formation may be directly from vapor or by freezing of supercooled water drops. The glaciation process may set in at different supersaturation as different ice nuclei may be present (see chapter 3 State of the Art). Nevertheless, even if ice formation sets in, the ideal case of reducing the supersaturation to 0% is not achieved. If not enough potential IN are present or the

temperature is too high for homogeneous nucleation the supersaturation stays high. The ice crystal growth is often suppressed inside clouds and therefore saturation stays above 100% or cubic ice with a higher vapor pressure forms first at lower temperatures [37].

1.2.2 Ice nucleation

Due to thermodynamics ice is stable below $273K$ at atmospheric conditions (fig.: 1.5). But the phase change from liquid water to ice is a kinetically hindered process. During the freezing process an ice nucleus needs to be formed. The freezing process may either occur homogeneously or heterogeneously. During homogeneous freezing in a water droplet an ice cluster forms in the liquid water. These small clusters form spontaneously in liquid water. Only if the cluster reaches a certain size, it is stable and it will grow until the whole water drop is frozen. This critical cluster size is temperature dependent. The colder the temperature the smaller is the critical cluster size. As this cluster formation is a statistical process homogeneous freezing of a drop ensemble does show a stochastic behavior. One may define the nucleation rate J as following:

$$\frac{\Delta n_{ice}}{N} = 1 - e^{-J_{hom}(T)\Delta t} \quad (1.1)$$

The value for the homogeneous nucleation rate at a given temperature can be calculated. The detailed theoretical description is accessible in Pruppacher and Klett [42]. The nucleation rate has a high temperature dependence, and therefore homogeneous freezing is only observed at temperatures below $240K$ at reasonable time scales. In the later case of heterogeneous nucleation suspended particles or molecules act as ice nuclei, later noted simply as IN. They lower the energy barrier to form an ice nucleus of critical size. The exact working principle of these IN on a molecular scale is only known for some bacterial proteins. Under atmospheric conditions there are different modes of heterogeneous ice nucleation shown in figure 1.7.

In deposition freezing ice is formed on the IN directly out of water vapor, while drops freeze upon contact with a particle in contact freezing mode. The last two modes are closely related. Immersion freezing is a process where an IN is in the water drop and will lead to freezing of this drop. The particle may either have entered the drop after a collision or was included in the drop formation process. That does not necessarily mean that this IN had acted as CCN in the drop formation. In comparison during condensation freezing the liquid water drop forms around the IN which acts also as CCN first and the formed drop freezes thereafter. Within the upper troposphere all these processes play an important role. Immersion freezing can be most easily modeled and was used in this work to study the ice nucleation activity of mineral dust aerosols. A detailed description of the ice formation is only given for immersion freezing here. The ice nucleation process in the immersion freezing mode has two principal model descriptions, the stochastic and the singular approach. Both models are applied on an ensemble of drops in the following description. The stochastic model is related to homogeneous freezing and based on a nucleation rate at a given temperature. The suspended IN has an intrinsic ice nucleating property. All particles/molecules behave the same way, i.e. have the same nucleation

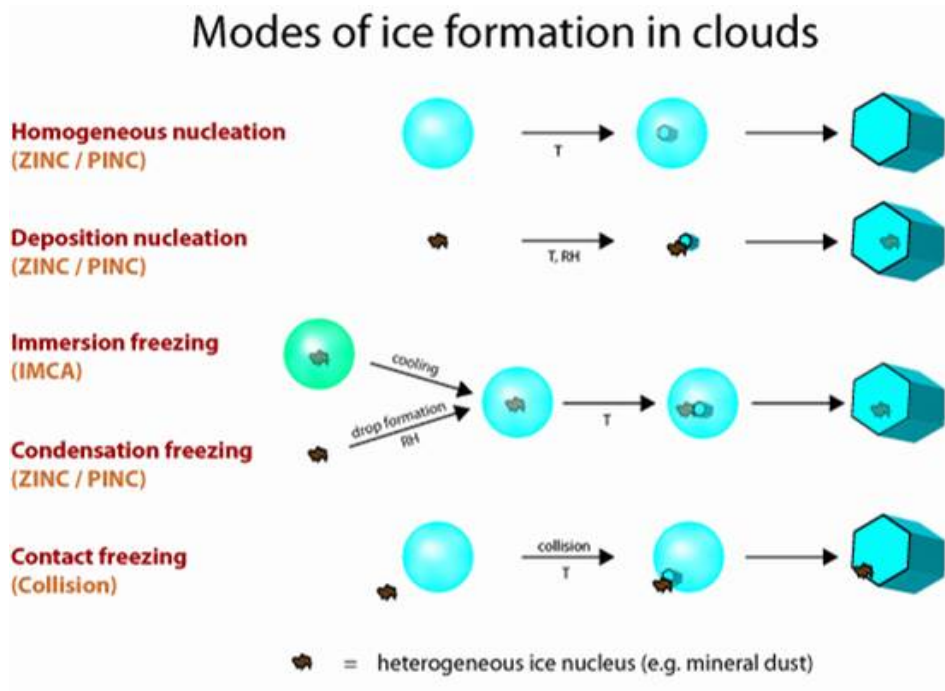


Figure 1.7: The different nucleation modes under atmospheric conditions. Image taken from ETHZ faculty for atmospheric and environmental science

site. The freezing of the drops is a purely stochastic process. The stochastic model leads to following equation

$$\frac{\Delta n_{ice}}{N} = 1 - e^{-J_{het}s\Delta t} \quad (1.2)$$

If different substances are inside the droplet which do nucleate ice. One can define equation (1.2) for every active component. It is possible to sum over all these IN, this will give:

$$\frac{\Delta n_{ice}}{N} = 1 - e^{-\sum J_i s_i \Delta t} \quad (1.3)$$

The stochastic approach can be well applied to well mixed ensembles. For complicated substances the singular model was developed. The singular approach describes the IN with specific nucleation sites. Every ice nucleating site on a molecule or particle will nucleate ice under a characteristic set of conditions. The site will become active at a given temperature upon cooling. The freezing process in the simple model is time independent, so once the site gets active it will freeze immediately. The active site density n_s is defined as the number of nucleation sites active at a given temperature per surface area. This approach leads to the equation for the singular approach of heterogeneous freezing.

$$f_{ice} = \frac{n_{ice}}{N_{tot}} = 1 - e^{(-n_s(T)s)} \quad (1.4)$$

The singular approach is also only an approximation, to obtain better results equation (1.4) may be adapted to the used cooling rates in the experimental set-up.

$$f_{ice} = \frac{n_{ice}}{N_{tot}} = 1 - e^{(-n_s(T-\alpha)s)} \quad (1.5)$$

The freezing process is thought to be always a stochastic process, but the time dependence in most cases is neglectable to the variety of the sample/experiment. As for homogeneous freezing the nucleation rates are highly temperature dependent i.e. no activity is observed even on a long time scale at higher temperatures than the one where the site is treated as active in the singular model. If the cooling rate is low enough for the system to respond, equation (1.4) can be used to characterize the ice nucleation activity of the IN properly.

Niedermeier et. al have developed more complex models to analyze ice nucleation [35]. The soccer ball model uses a new approach of treating different nucleation sites on particles. Niedermeier et al. use a finite number of different nucleation sites with a certain density per surface area in their approach. Each site has a characteristic nucleation behavior characterized with a contact angle, but the nucleation event on each particular site is a stochastic process (see Niedermeier et al. for more details [35]).

1.3 Atmospheric aerosols

The atmosphere is not a clean gas environment, but many aerosols are found there. The concentration of these aerosols have a high local and annual variability. The highest impact on the climate have water aerosols which form clouds, but water will be excluded in this section. Within the atmosphere primary and secondary aerosols are present. Primary atmospheric aerosols can be classified in different ways. Common classifications are anthropogenic and non-anthropogenic, inorganic and biological or anthropogenic, natural inorganic and natural organic. Primary aerosols are directly emitted as liquid or solid from various sources. The primary aerosols are emitted by anthropogenic combustion processes, physical erosion of rocks and natural dust areas, volcanic eruptions, biological organism or sea spray salt. Aerosols are suspended particles or drops in a gas, in this case the earth atmosphere. The aerosols may be formed by three different processes: drop particle conversion (dpc), bulk to particle conversion (bpc), gas to particle conversion (gpc) [42] Most aerosols are found in the lower layers of the atmosphere with estimated 80% up to 1km height [42]. The most abundant primary aerosols are: Sea salt (dpc), mineral dust (bpc) and burning products (anthropogenic/forest fires). Biological aerosol particles found in the are fungi, fungi spores, bacteria and pollen. The second group of atmospheric aerosols are secondary aerosols. They are formed by gas to particle conversion. Common secondary aerosols are sulfate, ammonium, and nitrate [39].

All this aerosol particles may act as CCN or IN. Pratt et al. had done a ice residual analysis [40]. During this experiment ice particles in the atmosphere were sampled on a flight over Arizona. The ice particles were analyzed with an aerosol mass spectrometer. With this setup the other compounds inside the ice particle could be determined.

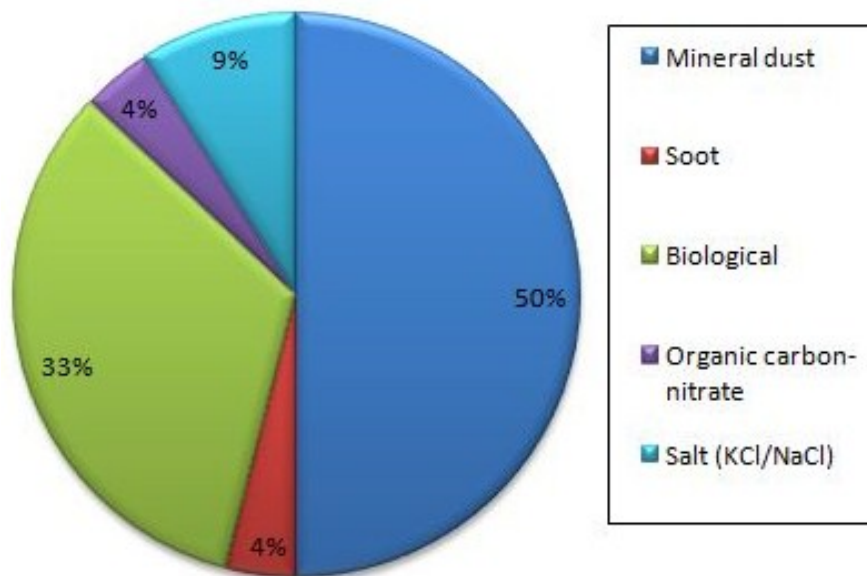


Figure 1.8: Chemical composition of ice-crystal residues. This was a single measurement over Wyoming with a aircraft - aerosol time of flight mass spectrometer. Figure taken from Pratt et al. [40]

This analysis of ice residues gave a different composition than the average background aerosol in this region. The values of this study are displayed in figure 1.8. Most of the ice residues are mineral dusts, biological material and sea salt. This ice residual analysis measures all particles inside (and on the surface of) the ice crystal. Thus, these particles did not necessary act as IN when the ice crystal was formed. Nevertheless, the biological fraction is rather high compared to background aerosol. Mineral dusts may also play an important role on ice nucleation. Pratt et al. suggest sea salt and organic carbon to play only a minor role in atmospheric ice nucleation [40].

It needs to be considered that the ice residues analysis by Pratt is a single measurement. But also data from other measurements like the 2004 flight measurements during the CRYSTAL-FACE campaign allow the same conclusions [7].

Heterogeneous ice nucleation on atmospheric aerosol particles is studied with growing interest [3, 34, 43, 54]. Artificial snow production has pushed the field further. The performance of different natural IN has been studied by many research groups. Ice nucleation activity of mineral dusts and bacteria has been studied for a long time. Freezing temperatures of natural dusts like Saharan dusts range from $255K$ to $235K$ [34]. Biological material is active up to the thermodynamic freezing point. Only a few single mineral ice nucleation experiments have been carried out in the past. A comparative study of minerals occurring in nature has not been made prior to this work. The ice nucleation experiments focused on natural samples containing considerable amounts of impurities. The process of ice nucleation on mineral dust particles is therefore not fully understood. Natural dusts have a quite complex composition, consisting of clays, quartz, feldspars,

calcite, gypsum and some others. The average composition of natural dust is shown in figure 1.9. Many of these minerals are thought to be able to nucleate ice. In chapter 2 the sample selection, based on natural sources and the average dust composition, for the ice nucleation experiments in this study is explained in detail.

As stated above there was no comparative study between different minerals prior to this work. In April 2013 Atkinson et. al published their work on the importance of feldspar for ice nucleation by mineral dust in mixed-phase clouds. They present a comparative study of different mineral phases [3]. The studied samples are quite similar to this work, but the work by Atkinson et al. gives no interpretation of the origin of the different ice nucleation activities of mineral dust particles.

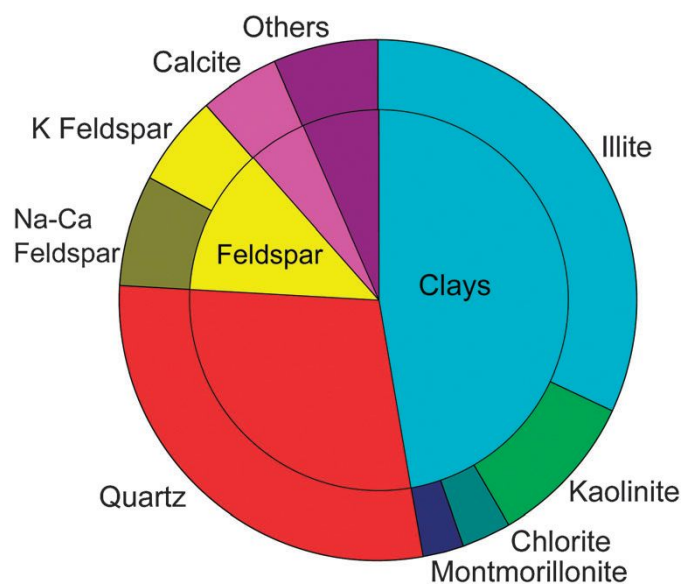


Figure 1.9: The average dust composition from different studies. Data taken from Murray et al. [34]

Experimental

2.1 Sample selection

The focus of this work lies on mineral dust particles and their ice nucleation activity. The selection of the samples is based on the average atmospheric dust composition. In the first series of measurements standard minerals were used to represent different components of natural occurring dusts (see figure 1.9). Calcite accounts for around 5% of atmospheric aerosol dust. The amount may be drastically increased in areas with limestone or dolostone mountains. $CaCO_3$ and $(Ca, Mg)CO_3$ are the main components forming these rocks. Limestone is a sedimentary rock mainly composed of $CaCO_3$ in the form of the minerals calcite and aragonite. Both minerals are weak against chemical weathering and physical erosion. Water has a recognizable solubility for $CaCO_3$ which decreases with pH. The slightly acidic rainwater due to CO_2 absorption dissolves part of the calcite. The weathering processes lead to the quite brittle nature of these rocks and to large amounts of rockfalls. As a result larger quantities of dusts are emitted by the limestone areas compared to other rock areas. Dolomite ($(Ca, Mg)CO_3$) forms the dolostone. This rock has almost the same properties as limestone if compared to most other rocks and was not studied in detail in this work. Technical calcite was used in the experiments to represent mineral components of limestone and dolostone.

There are not that large rock areas of gypsum on the earth surface, but acid rain weathering and other chemical erosion processes of calcite may produce enough particles of Gypsum that could be active in the ice nucleation process. Only a small amount of gypsum is present in the atmosphere as was shown before (fig. 1.9).

Silicates are the main rock forming minerals on earth. The silicates are geologically classified as rock minerals and clay minerals [17]. The first are formed intrusively or extrusively out of magma in the earth crust. This process occurs at high temperatures and pressures. The rock forming minerals tend to be a lot harder than the clays. Clays are weathering product of rock materials. The silicate clays are formed by chemical weathering of the silicate rocks. This process usually takes a long time, depending on the

Table 2.1: The samples of this study. The exact chemical composition will be given in the results section. The chemicals were purchased from 1) Sigma-Aldrich[®], 2) Alfa Aesar[®], 3) drugstore, 4) ICE-SAR ,Icelandic Association for Search and Rescue; 5) PTI- powder technology inc; 6) Fluka[®]

Sample	Chemical formula	Natural source
Calcite	$CaCO_3$	limestone and dolomite rock ¹
Gypsum	$CaSO_4 \cdot 2H_2O$	sedimentary rocks, hot springs ¹
K-Feldspar	$KAlSi_3O_8$	granite, gneiss, desert dust ²
Albite	$NaAlSi_3O_8$	granite, gneiss, desert dust ²
Andesine	$(Na, Ca)(Al, Si_3)O_8$	granite, gneiss, desert dust ²
α -quartz	SiO_2	granite, sandstone, desert dust ¹
α -quartz	SiO_2	granite, sandstone, desert dust ⁶
α -quartz	SiO_2	University mineral collection
Montmorillonite	$(Na, Ca)(Al, Mg)(SiO)(OH) \cdot nH_2O$	dusts ¹
Kaolinite	$(Al, Si)(O, OH)$	dusts ³
Volcanic Ash		volcanic eruptions ⁴
Arizona Test Dust	$SiO_2, K_2O, Na_2O, Al_2O_3$	Arizona desert ⁵
Limestone	$CaCO_3$	Gesäuse, AT

rock. For the ice nucleation experiments the most common rock and clay minerals were investigated. The best known silicate rocks are granite, gneiss and sandstone. Granite and gneiss are quite common on the earth crust. Granite is one of the most common ingenious rocks on the earth crusts. It is mainly composed of quartz and feldspars. In this study three different α quartz and three different feldspars (andesine, microcline and albite) were used. Feldspars, quartz and their weathering products are present in large amounts in the dust of the great deserts on earth like the Sahara, Gobi, North American deserts or the Australian deserts [34]. Uplifted dust from the great deserts accounts for more than 50% of the total eroded mineral dust particles [1]. As representative minerals for the desert materials the clay minerals montmorillonite and kaolinite and quartz were chosen. The investigated particles account for more than 70% of all silicate dust in the atmosphere.

Later also the ice nucleation activity of mixed natural samples was studied. Arizona Test Dust (ATD) is a standard dust sample, sampled in Arizona, US, which can be

purchased from the manufacturer (PTI). This sample is mainly composed of the silicate minerals listed above. A natural limestone was sampled at Hochtorn, Gesäuse, Austria to study the difference in IN activity in comparison to technical calcite. Volcanic eruptions are known to have a huge impact on the local and even global radiation and temperature balance. Ash particles may act as condensation and ice nuclei [48]. The used volcanic Ash sample is from the 2010 eruption of the Eyjafjallajökull, Iceland. It was sampled a few days after the eruption in April 2010 by local Icelandic association for search and rescue (ICE-SAR). A summary of all samples is shown in table 2.1.

2.1.1 Pre-processing

The samples were purchased either as whole rock grains or as milled powders from the manufacturer. The rocks were first crushed using a hard metal mortar. Thereafter the small grains were hand milled with an agate mortar and pestle. The milling time varied between the different samples. Milling was performed until the particle size was under $20\mu\text{m}$. The volcanic ash sample did contain some harder grains, so it was milled for 8 minutes in a hardmetal swing mill. In addition, the quartz and feldspar samples were milled to smaller grain sizes with the hardmetal swing mill for additional experiments. All milling processes were done under dry conditions.

2.2 Methods

The dust particles were analyzed using X-ray diffraction for bulk phase analysis. Electron microscopy was done to study the morphology of the particles. In addition EDX measurements were done to study the exact composition and its variability in the different grains of the samples. Finally some particles were also studied with transmission electron microscopy (TEM). Elemental mapping, Z-contrast, and high resolution images were recorded. Fourier transform infrared spectroscopy (FTIR) was used to study the surface and potential adsorbed molecules. The ice nucleation activity was studied in the immersion freezing mode with the emulsion method (see 2.2.4).

2.2.1 X-ray diffraction - XRD

All XRD measurements were performed at the TU Vienna X-Ray Center (XRC). XRD is a diffraction technique that can either be used for phase identification of solids or for structure determination. It is applicable to powders, films, and single crystals. Only bulk phases can be identified properly with XRD using the periodicity of the sample to get information. Therefore, only structure determination of periodic (crystalline) samples are possible.

Working principle

X-ray diffraction is based on elastic scattering of X-rays by electrons of the atoms within the sample. The incoming radiation is in a first approximation scattered at different

angles at the atomic positions. In fact the scattering rate is depending on the electron density of states for the different positions. For phase analysis the needed information can be reduced to the atomic positions. Therefore, in a first approximation the scattering is mainly occurring at the atomic positions by the well localized core electrons. The X-rays scatter at the electron shells, but XRD is only applicable in condensed matter. In 1913 Bragg proposed the Bragg diffraction model for diffraction of X-rays on periodic systems like crystals.

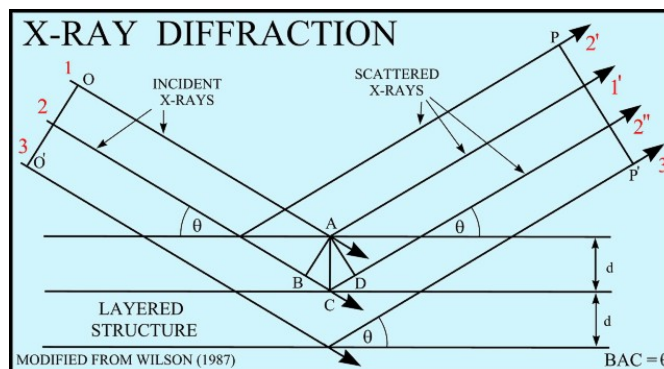


Figure 2.1: Scattering model of coherent X-rays on a periodic layered structure. The incident beams 1,2,3 are either scattered on the crystal plane or pass through. If the angle Θ does exactly fulfill Bragg's law, constructive interference of the resulting beams 1',2', 2'', 3' is observed.

$$2d\sin\Theta = n\lambda \quad (2.1)$$

In the XRD experiment a coherent beam of X-rays is used. The X-rays scatter at the atomic distances in all directions. If we consider just the linear model of figure 2.1 Bragg's law can be formulated for the outgoing radiation (eq. 2.1). Radiation interferes constructively if the beams are of the same wavelength and phase. For elastically scattered X-rays the wavelength does not change in the sample, but the phase. The phase change of electromagnetic wave is a periodic function [31]. If the path difference that the two incident beams have to travel is an integer multiple of the wavelength (λ) they are in phase after the diffraction process. The distance between a specific set of crystal planes (d) is a material specific quantity. Crystal lattice planes can be defined by the Miller indices (h, k, l). Specific planes will not show reflectance depended on the symmetry of the crystal. The wavelength in the Bragg's equation is determined by the used light source. If source and detector are at the same angle Θ relatively to the crystal plane the beams interfere constructively. If equation (2.1) is fulfilled constructive interference is achieved. In powder XRD a powder is used as sample. The powder grains are usually randomly oriented in space. The grains have different crystal plains facing the radiation source. If the angle between the sample and the source is varied constructive interference is always obtained when Bragg's law is fulfilled for a specific crystal plain. The resulting diffractogram gives intense peaks at different angles which are called reflects. The diffractogram has a structure specific appearance. The intensities of single

peaks depend on the scattering rate on the electron shells i.e. the atoms in the sample. The peak position just gives structural information. With a refinement of the measured diffractograms phases can be identified. This formulation of Bragg's law is a real space description and in some sense an approximation, but well enough for the phase analysis with XRD data banks used in this work.

Powder X-ray diffraction

In powder X-ray diffraction, powders which grain sizes around $1\mu m$ can be easily analyzed. The powder is placed on a steel sample holder and then inserted into the X-ray diffractometre. In the used routine measurement the angle was varied between 5 and 120° . The obtained diffractograms can be compared to millions of diffractograms of substances which are available in databases. For most compounds reference measurements with a standard are available. The intensity ratio of a specific peak of the reference compound and a peak of the compound is accessible in the data base. That way a semi quantitative phase analysis of the powder sample containing indexed phases is possible. If data was available this was done for the used mineral samples. As X-ray source the copper K_α line was used in all the experiments. All samples were used without further treatment prior to the XRD experiments except milling. The measuring time varied between 1h for the single mineral samples and 3h for the natural samples. Diffractogram analysis was done with the Powder Diffraction File (PDF) data base and the HighScorePlus software.

2.2.2 Fourier transform infrared spectroscopy - FTIR

Infrared spectroscopy

Molecules have three different degrees of freedom in space: translation, vibration and rotation. The energy for vibrational transitions for a single vibration of a bond is given by equation (2.2)

$$\nu = 1/2\pi\sqrt{k/\mu} \quad (2.2)$$

where k is the force constant of the bond and μ is the reduced mass of the atoms. Vibrational transitions lie energetically in the range of infrared light. Infrared spectroscopy may therefore be used to identify structures of compounds. The traditional dispersive technique (scanning technique) measured the absorption of a single dispersed wavelength at a time. During the measurements the selected wavelength was varied and the spectrum obtained. Since the seventies Fourier transformed infrared spectroscopy is applied. Instead of monochromatic light the polydisperse IR radiation is shined on the sample. An interferometer is placed in front of the sample. Through Fourier transformation of the light intensity signal a spectrum can be calculated. The interferometer working principle is the interference of coherent light. The light of the source is split by a semitransparent mirror in two parts. The light reaches another mirror and is reflected. At the beam splitter the two beams are again reflected or transmitted. Depending on

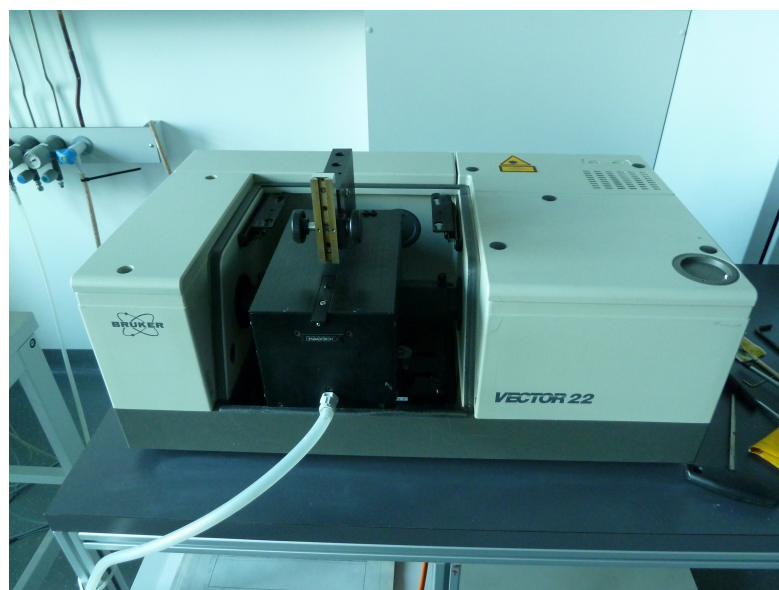


Figure 2.2: The used Bruker Vektor 22 for the FTIR analysis

the length of the travel path and the wavelength of the radiation they interfere constructive or destructive. Constructive interference is obtained if the path difference equals an multiple of the wavelength. In an FTIR measurement setup, one of the two beams is moveable. During the measurement its position is changed and the light is measured at the detector. In general a laser is used to measure the mirror position. The obtained interferogram is then Fourier transformed into an IR-spectrum. FTIR has two main advantages, noted as Fellgett and Jacquinot, over the dispersive technique. The intensity of the radiation is increased as the beam is not dispersed leading to a better S/N ratio. The latter, also known as throughput advantage, leads to a larger optical throughput as FTIR spectrometers have no slits where intensity is lost.

FTIR measurements can either be performed in transmission or reflectivity mode. In transmission mode the beam passes through the sample and its intensity loss is measured. In Diffuse Reflectance Infrared Fourier Transform Spectroscopy (DRIFTS) the diffuse reflectance of the sample is measured. In comparison in Attenuated Total Reflection (ATR) the sample is placed on a crystal. The incident beam is total reflected in this crystal, but due to the continuity of the wave function it is extended to the sample. This evanescent wave may interact with the sample. If the sample absorbs part of it the total reflected beam is lower in intensity. ATR-FTIR is faster and no transparent sample is needed. The FTIR study of the mineral samples was done on a Bruker Vector 22. Germanium was used as ATR-crystal. At least 1000 scans were performed per sample to get a better S/N ratio. Post processing of the IR-data was done with OriginPro 8.5.1.

2.2.3 Electron microscopy

Scanning electron microscopy (SEM)

Electron microscopy uses an electron beam for scanning. The beam is creating different responses of the sample, which are used for imaging. There are different imaging possibilities depending on the used signal like X-rays, back-scattered electrons, or secondary electrons. In scanning electron microscopy the electron beam is moved around the sample surface. The resulting signal at the detector is connected with the corresponding position on the sample. The image is not online but created by scanning over the sample area. The contrast in the image depends on the used imaging technique. The signal intensity depends on the atoms present in the sample and the morphology of the sample. The intensity of the secondary electrons for example is depending on the angle of the incident beam, giving a contrast for different orientated faces. A real space image is calculated using the intensity/position pairs. The spacial resolution of secondary electron scanning electron microscopes is rather high. The resulting image has a three dimensional appearance even on low scale, due to the narrowly focused primary electron beam. To obtain (good) images the sample need to be electronically conductive. Insulating materials are often coated with novel metals or graphite. A resolution up to the nanometer range is achieved. The whole instrument is under high vacuum.

The EDX measurement is based on the detection of the characteristic X-ray radiation emitted by the atoms in the sample. The initial electron beam hits the sample and secondary electrons are removed from it. This can be used for imaging processes. The secondary electron, created, leave electron holes on the atoms, which are filled with electrons from higher states. The emitted X-rays are measured with an energy dispersive detector. The X-rays are element-specific. Microprobe EDX can be used for elemental mapping and local quantification of elements. Quantification of elements with large differences in atomic number becomes less accurate. The emitted X-rays are partly absorbed by the heavy atoms or in cavities on rough surfaces. For very light elements the quantification is rather difficult, due to a higher absorption of the soft-X-rays. In the studied samples the oxygen content of the mineral dusts could not be determined accurately with EDX. Hydrogen is not accessible at all with this method. The error of the used EDX lies around 0,5% for the trace elements and 1% for the main components, except oxygen.

SEM measurements were performed at the USTEM at Vienna University of Technology. The mineral dust samples were put on a graphite plate. The particles were sputtered with the AuPd 30s 15mA (4nm) program. This leads to a 4nm AuPd coating to make the sample conducting and avoid charging which would disturb the imaging process. After coating the samples were inserted into the microscope. Images with 1000x, 10.000x and 20.000x magnifications were taken. The experiments were performed with the FEG-SEM device, which also has the possibility to do EDX measurements.

Transmission electron microscopy (TEM)

The TEM is an electron microscopic technique that measures in the transmission mode. The initial electron beam is created at a tip, which is typically made out of tungsten, by applying a very high voltage. The electrons are focused with a lens system to a convergent beam. Upon transmission the electrons may interact with the sample and are recorded on a detector. This is either a phosphorous screen or based on a CCD-camera. The used TEM equipment at the USTEM was also capable of measuring in STEM and SEM mode. In the STEM mode a EDX mapping is possible. The electron beam is focused locally for STEM measurements.

TEM/STEM measurements were done on the feldspars albite and microcline. Classical TEM images and Z-contrast images were recorded on different sample grains. On the features visible in the Z-contrast images EDX measurements were performed. EDX-mapping was done over morphological features like cracks.

2.2.4 Cryo- microscopy

Cryo-microscopy is used to study immersion freezing. It is based on an optical light microscope. The ice crystals are detected by a change in reflectivity since for frozen drops it is lower than for the liquid ones. The cryo - microscope setup can be seen in figure 2.3. The reaction chamber consists of a Peltier based cold stage. The used TES2-31-17-20 Peltier has three stages with many semiconducting units. In the thermoelectric cooling device the heat is transported from one side to another by an electric current. The reason lies in the different work functions of these solids. In a thermo element two different materials (i.e.: differently n/p-doped semiconductors) are in contact resulting in a contact potential. If two such junctions are at different temperatures a voltage can be measured which is temperature dependent. This effect is known as Seebeck effect and can be used to measure temperature. In an thermoelectric cooling device the opposite Seebeck effect, the Peltier-effect, is used. If a voltage is applied, heat is transported from one side to the other. The transported heat is dependent on the used thermo-element and the applied current (eq.: 2.3). In a thermoelectric device multiple thermo-elements are connected in series to optimize the cooling effect.

$$P = \frac{\Delta Q}{\Delta t} = \pi I \quad (2.3)$$

The cryo - microscope setup consists of a TES2-31-17-20 three stage Peltier-element. During cooling it is operated with a laboratory power supply device where the current is varied. The Peltier stage is directly connected to a temperature measurement device of type PCE-T312 thermometer. It is cooled with water of $12 - 15^{\circ}C$ by a pump system. The whole element is placed in a Teflon box. Its accuracy is higher than $\pm 1K$. The box can be flushed with nitrogen or other gases to remove water from the cell. This could otherwise interfere the measurement. At top of the box is a glass window, which enables the observation of the experiment with an optical microscope. The whole „cryo-cell“ setup was designed at the Vienna University of Technology. It was placed on

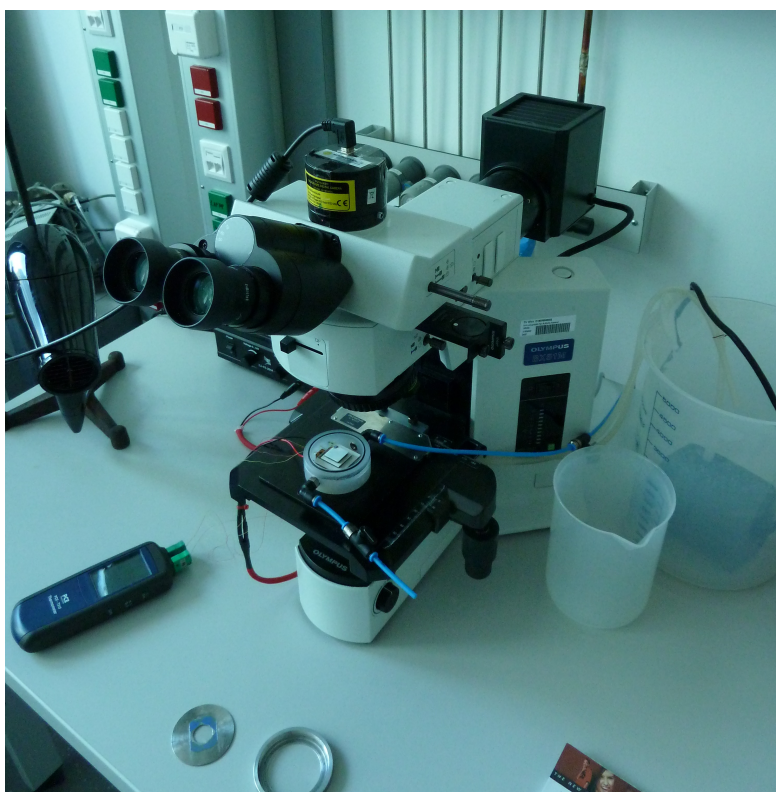


Figure 2.3: The cryo- microscope that was used for the immersion freezing experiments. The cryo cell is open on the picture. Cooling is achieved via two tubes and a pumping system in the large beaker to the right. The blue tube is connected to a Nitrogen source to flush the cryo-cell. The microscope camera MDC-200 is on the top. Data can be directly accessed via USB. The hairdryer on the left was used to avoid a blushing of the cell window.

a microscope. The used microscope was an Olympus BX51M. A MDC-200 microscope camera was used to record images of the samples during experiments. The used software for the camera was ScopeTek minisee Version x86, 1.1.333.

Experimental procedure

With the cryo - microscopic setup ice nucleation in the immersion freezing mode can be studied. Therefore an oil - emulsion method was used, where water was mixed with oil. The oil consisted of 85wt% paraffin and 15wt% lanolin (water free). After proper mixing a small drop was placed on a cleaned cover slip. The cover slip was then placed into the cryo-cell onto the cold stage. The cell was closed and flushed with nitrogen for about 2min. The applied current was manually increased slowly. With the camera-microscope setup images were taken if changes arose. The corresponding temperature was also recorded. All measurements ranged from 278K to 228K. Images were recorded when a change in the image was observed or every full degree below 253K.

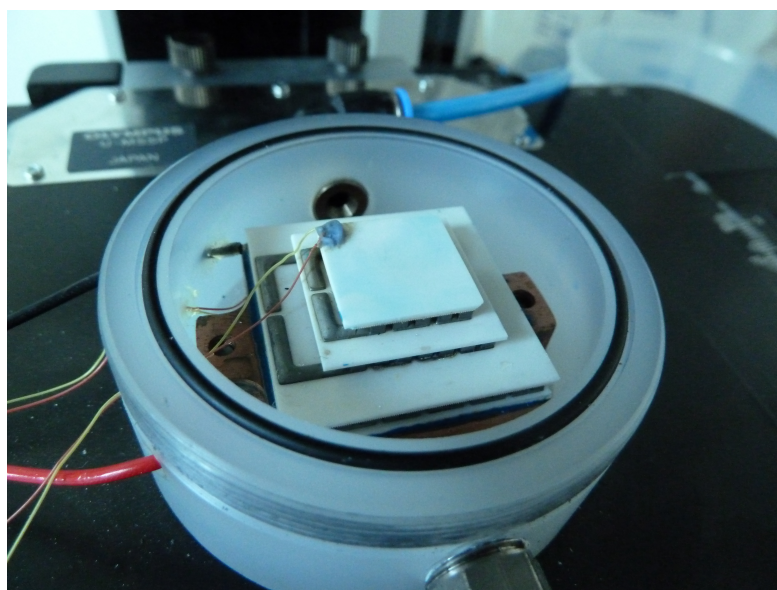


Figure 2.4: This is a close up of the cryo-cell. In the center is the white Peltier cooling stage. The thermometer is connected with the thin red/yellow wires. In the back is the blue nitrogen tube inlet. The water cooling of the Peltier-element is not visible here as it is below the Peltier-element. The cell is open on the image.

Data analysis

The optical properties of water change upon the phase change from liquid to solid. The frozen drops therefore appear darker in the image than the unfrozen ones (fig.: 2.5). This is a relative effect so only a change can be quantitatively analyzed. The amount of newly frozen drops was counted for each image/temperature and summed up. This way freezing curves were obtained. The measurements were all performed until no more drops froze or $228K$ was reached. The resulting freezing curves were summed up if statistically allowed. Missing frozen fraction points at temperatures of the other measurement were interpolated linearly. In the results section of this work median freezing temperatures are reported. This represent the median value of 50% frozen drops. Deviation values were obtained from 33% and 66% values. All values were rounded to integer values. A typical plotted freezing curve in the results section consists of minimum two independent measurements and four different cooling runs (compare fig.: 4.8. The number of counted drops, plotted per curve, are always more than 250 giving a appropriate statistics. The measurement uncertainty of the cryo -microscopy is $\pm 1K$ given the same value for the freezing curves. Median and deviation values were always rounded to integer values.

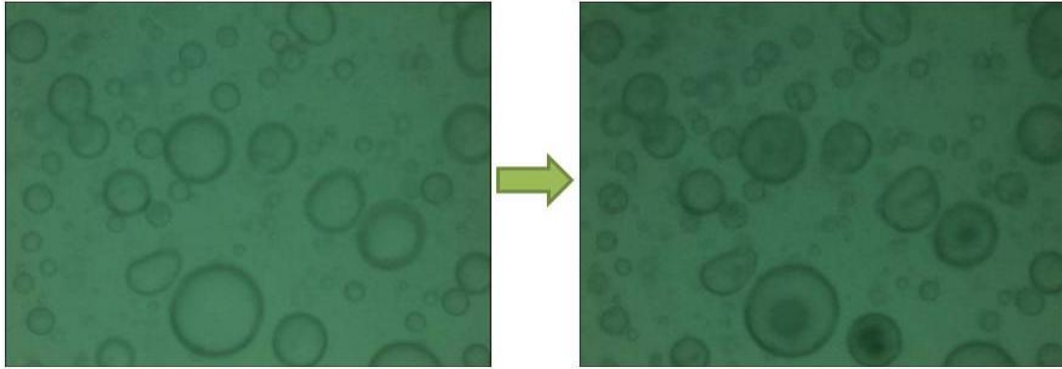


Figure 2.5: Upon freezing the drops do change their optical properties. Frozen drops appear darker in the microscopic image.

2.3 Sample preparation

The used samples were all pre-milled to particle sizes of around $1\mu\text{m}$, see section 2.1.1. For the standard immersion freezing measurements 20mg of the mineral dust were suspended in 1ml ultra pure MilliQ[®] water. After mixing $1,2\text{g}$ oil ($85\text{wt}\%/15\text{wt}\%$ paraffin/lanolin) were added, resulting in a $45 : 55\text{wt}\%$ ratio of water and oil. A concentration of 20mg/ml dust particles were used as this was the lowest concentration that did not show lots of homogenous freezing for most samples. The so prepared emulsion was mixed and in some cases treated in the ultra sonic bath to obtain a better mixing. For the measurement a drop of around $4 - 8\text{mm}$ was placed on a cover glass and inserted into the cryo - cell (see section 2.2.4).

The surface area of the quartz samples and montmorillonite were measured using a BET setup. The surface areas of the other mineral dusts could not be measured as too few material was available. The surface area of those minerals was estimated based on the SEM-images.

Heat treatment

If heat treatment was applied on the samples, it always refers to a heat treatment of the dust particles in an oven. There were two different types of heating applied, wet and dry. In the dry case, the particles were placed into a ceramic bowl and covered with aluminum foil with small holes in it. The bowl was then inserted into the oven. The sample was either constantly heated at 373K or 523K or with a temperature program for four hours at 773K . For wet heat treatment the particles were first suspended in MilliQ[®] water. The suspension was filled into the bowl which was placed in the oven. Approximately, every hour a small amount of MilliQ[®] water was added. The low temperature oven was a steel lab oven with a temperature range of $320 - 570\text{K}$. The high temperature heating was done in an ceramic oven. The typical temperature program had a heating time of 1h

up to 773K. The temperature was kept for four hours at 773K. After cooling down the particles were stored in plastic viols or used directly for nucleation experiments in both cases.

Enzymatic treatment

It is possible that ice nucleation activity on mineral dust particles is due to adsorbed biological material. To investigate that cause the particles were treated with different enzymes. For this treatment a water particle suspension was made. Concentrations varied between 20 and 50mg/ml. The frozen enzymes were added to the suspension. The solution was then heated to the working temperature of the used enzyme in a water bath. The reaction time was 3-5hours. The used enzymes are listed in table 2.2. Papain and Pronase E are protein digesting enzymes. Pronase E does cleave enzymes between two hydrophobic amino acids, like Ala, Val, Leu, Ile, Phe, Trp, Tyr, Papain at an Arginine or Lysine site [46]. Onozucka destroys polysaccharides and Lipase destroys lipids.

Table 2.2: The enzymes used in this study with their corresponding working temperatures

Enzyme	used concentration	Working temperature	Manufacturer
Papain	2mg/ml	340K	AppliChem [®]
Pronase E	2mg/ml	310K	Merck
Cellulase Onozucka	5mg/ml	310K	Merck
Lipase	2mg/ml	308K	AppliChem [®]

Washing water

To study soluble IN on the particles a washing water was produced. Therefore, the particles were suspended in MilliQ[®] water. The suspension was mixed on a regular basis and after an incubation time of 8-15h the particles were removed. The suspension was centrifuged at 3000RPM for 40 minutes in a lab centrifuge. The top water was then taken for immersion freezing measurements. The used particle concentration to produce the washing water was always 20mg/ml particles.

State of the art

The investigation of ice nucleation on inorganic particles has a long history. Mineral dust particles were found in snow residuals already in the 1960ies [25]. Over the years different aerosol techniques were applied to study their ice nucleation behavior. Mineral dusts were found to be capable of nucleating ice [42]. Nevertheless, most studies focus on natural dust samples, which often have a quite complicated and mixed composition. Natural occurring mineral dust particles are almost always a mixture of different minerals. It is appropriate to study the ice nucleation behavior of natural occurring dusts from the atmospheric point of view. Nevertheless, better defined samples are needed to get a deeper insight into the ongoing nucleation processes. In the last decades the amount of techniques available to study ice nucleation increased. Industrial interests in artificial snow generation at higher temperature and improvements in biological IN studies pushed the field further [43].

Inorganic particles, in particular mineral dusts, may act as IN. The exact mechanism of heterogeneous ice nucleation on dust particles is not known for most minerals [34]. As there are many different experiments to study the ice nucleation activity, results are often hard to compare. Surface density of active sites (n_s) is not given for all experiments, but maybe be calculated. n_s values are a possible way to compare different studies of the ice nucleation activity [34]. As mentioned in chapter 1 the largest sources of mineral dust particles injected into the atmosphere are the great deserts, the focus of prior studies lies on desert dust and its main components. These are feldspars, clays, and quartz, but for most minerals appropriate single mineral measurements are lacking [34]. In general, it is quite hard to find pure single minerals from a natural source and also synthesis thereof is often a quite complicated process.

Different nucleation modes could be accessible with the various techniques ranging from air flow chambers to oil-emulsion microscopic setups. Most studies were performed on clay minerals (see below). Kaolinite is the clay mineral which was studied the most [28, 33, 38, 52]. Kaolinite shows ice nucleation activity in immersion freezing mode above $243K/-30^\circ$. Murray et al. report a data set of $241-243K$ median freezing temperatures

for kaolinite particles in the immersion freezing mode at concentrations of $1\text{wt}\%$ [33]. This is in agreement with Pinti et al. [38] who found freezing temperatures around 240K depending on the particle concentration per droplet used in their experiment. In addition they report a second nucleation peak at higher temperatures only found for Kaolinite purchased from Sigma aldrich[®]. The reason for this activity is not totally clear as no information about prior treatment and impurities in the samples was provided by the manufacturer. These two experiments used a quite similar experimental set-up as the one used in this study. Pinti et al. uses calorimetric measurements to follow the freezing processes of the emulated droplets [38]. L  ond et al. performed continuous flow chamber experiments [28]. The nucleation temperatures, measured, are within the same range as the emulsion measurements mentioned above.

Montmorillonite samples were analyzed by Pinti et al. and Prubbacher et al. [38, 42]. While Pinti et al. found low ice nucleation activity at temperatures below 240K , Prubbacher et al. together with Hoffer report ice nucleation activity around 250K , but in the latter also the freezing temperature of pure water was much higher than 235K [16, 38, 42].

Pinti et al. further studied ice nucleation of illite. Freezing was observed around 245K . With higher concentrations the freezing curves are quite broad, they report heterogeneity of and impurities in the sample to be the reason for that [38]. Further Hoffer reports ice nucleation up to 249K for illite [16]. Both authors report a complex sample with more than one mineral. The illite used in Pinti's study contains $5 - 10\%$ kaolinite and calcite and trace amounts of feldspars and quartz. Hoffer has not given an exact quantification of the minerals.

Pinti studied all common clay materials using the same method. He found illite to be the most active IN followed by kaolinite and Montmorillonite [38]. Nevertheless, the illite sample contained other minerals, which may influence ice nucleation in favor of higher nucleation temperatures. Zimmermann et al. did aerosol water interaction studies [56]. Different ice nucleation behavior of the various mineral dusts was observed. They detected the freezing using an environmental electron microscope. The humidity in the reaction chamber at each measured temperature was increased stepwise. With this setup only the deposition mode was accessible. Even though they studied deposition ice nucleation mode the results may be of interest for immersion freezing measurements, as this study give a good comparison between different minerals. The ice nucleation activity of closely related materials, like the feldspars, was rather different. In fact microcline (K-feldspar) needed the lowest supersaturation at 261K to initiate ice formation. The species which were active at the lowest supersaturation were kaolinite, illite, hematite and microcline. kaolinite and hematite activated at quite high temperatures. This study was the first comparative study of the most common minerals present in atmospheric aerosol particles [56].

Klier et al. reported ice nucleation on silica material already in the 1970ies [22]. They tried to address the exact formation of ice. They suggest that the ice nucleation is a result of water molecules binding to the surface hydroxyl groups of the silanol groups [22, 45]. The performance of a silica/silicate material in ice nucleation may be

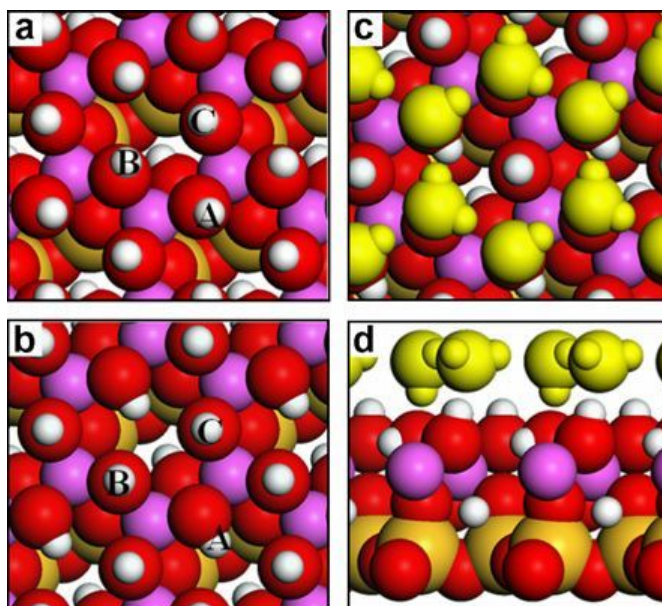


Figure 3.1: Computational simulation of an ice layer on a perfect kaolinite surface by Hu et al.. The hydroxylated kaolinite (001) surface is shown in the left images. The relaxed surface is on the lower image (b). The right images show the adsorbed water molecules in an ice-like structure by a top and side view. The atoms of the kaolinite structure are silicon (orange), aluminium (purple), oxygen (red), and hydrogen (white). The water molecules in c,d are marked yellow. Graphics modified from Hu et al. [19].

influenced by other atoms. In the studied micas fluorine atoms are reported to be quite important for the ice nucleation process [45]. The fluorine on the surface acts as active center for ice growth. The fluorine atoms are able to sustain elastic distortions in the growing ice lattice. They further suppose that the potassium atoms on the surface and those released into the surface bilayer have no negative impact on the ice nucleation while ions with higher charge density like Al^{3+} do so [45].

Eastwood et al. did a comparative experiment in the deposition mode [9]. kaolinite and muscovite were found to be good IN, while the quartz and calcite were poor. Montmorillonite was found a good IN below a certain temperature around $241K$. They conclude that the better performance of kaolinite and muscovite is due to better crystallographic match between the mineral surface and the hexagonal ice. kaolinite surface OH groups have a pseudo-hexagonal arrangement which enables a easier bonding to the hexagonal ice structure [9, 42]. Latest computational studies by Hu et al. [19] addressed the adsorption of ice monolayers on kaolinite (fig. 3.1). They found that the ice structure is stabilized on top of kaolinite. Flexibility of the surface atoms and the amphoteric nature of the surface support the ice structure together with a good matching of the amphoteric sites. The surface is able to sustain hydrogen bonds to the ice structure. Surface hydroxyl groups act as hydrogen donor and surface oxygen atoms as hydrogen bond acceptors. The hydrogen bond acceptors are flat lying hydroxyl groups. In the

pseudo hexagonal arrangement of the surface hydroxyls every second has the hydrogen atom horizontally in the surface and can therefore act as the acceptor (see figure 3.1). The flexibility of the surface hydroxyls leading to an amphoteric nature is another key parameter to stabilize the ice structure [19]. Even though Hu et al. report an ice layer stabilization on a perfect kaolinite surface, kaolinite is not a good IN as mentioned before [28, 33, 38]. Natural kaolinite may incorporate Na^+ or Cl^- ions on the surface to avoid dipole formation interfering the above mentioned processes [20].

Most studies concerning ice nucleation on mineral dust particles are based on natural dust samples. These samples vary from totally natural ones like Saharan dust or relatively well characterized test samples like ATD. Those are still natural samples, but they are well manufactured and therefore the results of different research groups are easier to compare. Most of these dusts are mixtures of the different clays mentioned above, quartz and feldspars. The composition varies largely. ATD is the most used proxy within the field. Initial freezing is reported around $249K$ [6]. This data is from an air flow chamber measurement at the AIDA in Karlsruhe. The other natural samples, namely Saharan and Asian dust in this study, were less active, but are able to nucleate ice. Knopf and Koop studied ATD particles using an optical microscope [23]. The particle stage was cooled to different temperatures and exposed to different relative humidity. The particle size was between $0.7-10\mu m$. The particles inside were exposed to increasing relative humidity until freezing was observed. They observed quite different nucleation temperatures for the particles. ATD particles nucleate ice in the deposition mode up from almost $258K$ on, but only a tiny fraction of the total particles are able to nucleate ice. This suggests that the ATD sample is quite inhomogeneous. The sample can be seen as externally mixed ensemble. The different minerals ATD is composed of have different ice nucleating properties. Most grains contain only one mineral. The results indicated also that the mixed ATD sample may also differ in its composition with particle size [Welti personal communication].

Welti et al. did show a particle size dependence of the ice nucleation activity [53]. The nucleation temperature in the immersion freezing mode decreases with smaller particle size [12, 53]. The relation was almost linear for the single mineral samples of kaolinite. While ATD did not show this behavior. It is assumed that the better IN are not found in the lower size fraction in the ATD sample. This active compound is not yet found, recent studies by Atkinson et al. would suggest K-feldspar to be the most active component in ATD [3]. Even the worst mineral IN seem to be able to nucleate ice under less humid conditions than homogeneous freezing.

Volcanic ash is known to be able to nucleate ice [48], but its composition varies from place to place and eruption to eruption. As for all natural samples, it is therefore of interest which particles serve as active nucleation centers in volcanic ash. Ash from the 2010 Eyjafjallajökull Volcano on Iceland was studied in the AIDA chamber. Freezing in the immersion mode was first observed at $252K$. At $249K$ only 0.1% of the particles are active in that mode. Volcanic ashes contain many different particles, but the immersion freezing performance in their measurement was worse than for ATD. It is assumed that the ATD sample contains more of these highly active particles than the volcanic ash.

The overall efficiency for volcanic ash is lower than for most natural dusts, but its onset freezing behavior is quite similar [48]. In comparison to pure kaolinite samples volcanic ash seems to have higher ice active surface density. The exact composition of the volcanic ash is not given in their work, in addition no surface analysis was performed. As volcanic ashes are in contact to sulfuric gases and acids a partial sulfate coating could occur. It was shown by [32] that a coating may reduce ice nucleation activity by reducing the active surface. However, Knopf and Koop found no quantitative difference in SO_4^{4-} coated and pure ATD [23]. Hoyle et al. studied volcanic ash of the same eruption [18]. They found high evidence that there are few IN present which are active at higher temperatures. These IN are highly active, but most of the „bulk“ dust is only active in the immersion mode 3–4K above the homogeneous freezing temperature. They performed two different measurements, a DSC immersion freezing experiment which was sensitive to the best IN present, while the IMCA/ZINC studies the properties of the particle ensemble. They had found lower freezing temperatures than for ATD with both methods. The overall impact of volcanic ashes to the ice nucleation on a longer time scale might be neglectable. Hoyle et al. found that the concentration of good IN 1-2days downwind are too low to influence atmospheric water vapor or cloud formation [18]. The high variability of ice nucleation activity within the volcanic ash sample from Eyjafjallajökull could be further expanded to older ice nucleation results. Hoyle et al. mentioned three possible influence of volcanic ash on ice nucleation behavior of the atmospheric aerosol ensemble as volcanic ash of different eruptions had been found to be a source of good IN, a rather bad IN not being able to nucleate ice at higher temperatures, and may even deactivate background IN [18]. Magma and as a result lava and ash composition is changed and can be regionally quite different.

In their study on clay minerals Pinti et al. further investigated Hoggar mountain dust, which is characteristic for Saharan dust. The exact composition was not analyzed. While its nucleation activity was higher than all clays in that study it was far less efficient than ATD. The Hoggar mountain dust and the illite came closest in ice nucleation behavior. This was in good agreement as the mountain dust is thought to contain high quantities of illite. The natural dust contained more good nucleation sites as the best site median freezing temperature was the highest for this sample. Together with Saharan dust concentrations above Cap Verde and the number density of best nuclei in the mountain dust, Pinti et al. suggest that enough IN are present to nucleate ice between 250 and 260K. They further mention that different interlayer cations may influence the ice nucleation process [38].

In recent studies a lot of biological material was investigated in ice nucleation experiments. There are biological particles that nucleate ice at much higher temperatures than mineral dusts [40,43]. Biological ice nucleation activity is limited to specific species. The total abundance of biological material is a lot lower than for mineral dust, but as shown in section 1.3 the amount of biological material is increased in ice residuals compared to background average aerosol. It was thought for a long time that most biological particles like pollen grains or certain bacteria are too large and too heavy to reach most cloud regions, and therefore, even if they nucleate ice, may not play a role in cloud glaciation. It

was shown by Pummer et al. that the ice nucleation active part is not the particle itself but soluble surface molecules [43]. These molecules can reach the upper troposphere. Mineral dust particles are thought to be potential carriers for those molecules. Mineral dust particles which have no intrinsic ice nucleation activity may act as IN at higher temperatures due to these adsorbed molecules. Verification of this effect is still lacking, but the opposite was observed. Active mineral dust particles in particular ATD became worse IN if covered with secondary organic aerosols (SOA) [32]. A full coverage of the surface reduces the ice nucleation activity drastically.

Results

Mineral dust particles were measured in the immersion freezing mode using the cryo-microscopic setup explained in the methods section (2.2). The particles had been milled to a grain size of $1 - 10\mu\text{m}$ diameter. Aqueous suspensions were made with a particle

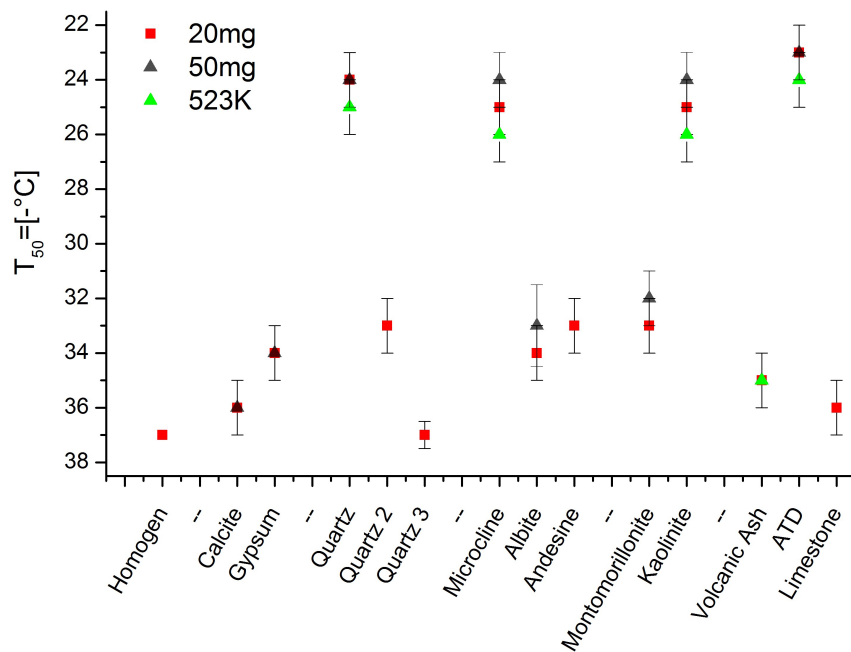


Figure 4.1: Ice nucleation results for all measured samples. The median freezing temperatures are displayed. The bars are the 33% and 66% fraction of frozen drops. The concentration of the mineral dust particles were 20mg/ml (black) or 50mg/ml (red) respectively. Heat treated samples are displayed in green. The different mineral classes are from left to right calcite+gypsum, quartz, feldspar, clays, and mixed natural samples.

concentration of 20mg/ml and 50mg/ml . The ice nucleation results for these samples are displayed in figure 4.1. The median freezing temperature represents the temperature where 50% of the drops were frozen (see section 2.2.4). The bars are obtained with the 33% and 66% values. With this experimental setup the median freezing temperature for homogeneous freezing of pure water is 236K shown on the very left in figure 4.1. Calcite can be considered as being not an active IN, as the homogeneous freezing temperature is within the error bars. Gypsum, montmorillonite, the volcanic ash sample, andesine (Na-Ca-Feldspar) and albite (Na-feldspar) are active IN, but at quite low temperatures. The initial freezing temperatures are around $243\text{K}/-30^\circ\text{C}$ with the median freezing slightly at colder temperatures. Most of these samples were not further studied in respect of their ice nucleation activity.

Obviously, quartz, microcline (K-feldspar), kaolinite and ATD seem to be good IN. They are active up to temperatures around $253\text{K}/-20^\circ\text{C}$. All the active dust particles were heat treated prior to the cryo-microscopic measurement. Firstly it was assumed that some adsorbed organics could be the origin of the IN activity. The ice nucleation activity was almost as good after the heat treatment (see green triangles in figure 4.1).

4.1 Non silicate materials

4.1.1 Calcite

The ice nucleation behavior of a technical calcite and a natural Limestone (Gesäuse, Austria) was measured. The FTIR spectrum is a pure calcite. The bands are the asymmetric (ν_3) and symmetric stretching (ν_1) of the C-O bonds in the carbonate at 1400 and 1091cm^{-1} , the out of plane C-O bending (ν_2) at 871cm^{-1} and the in plane bending (ν_4) at 711cm^{-1} [4].

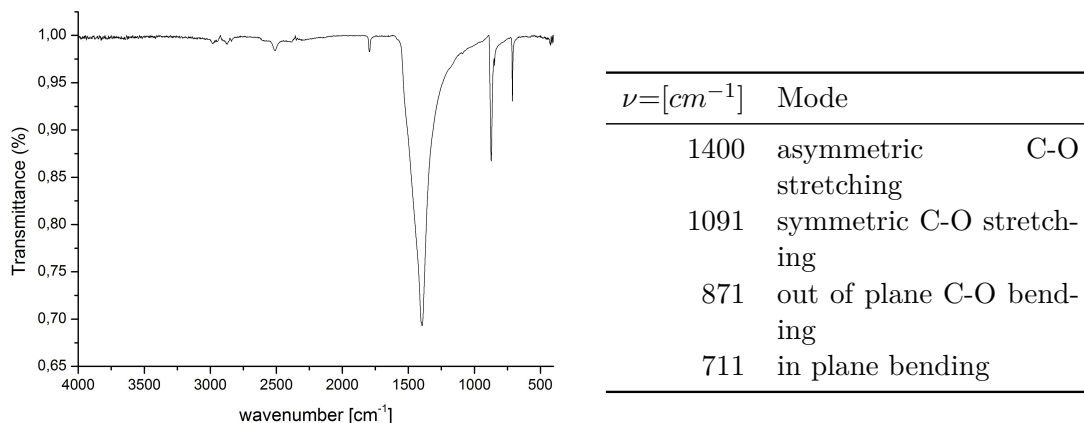
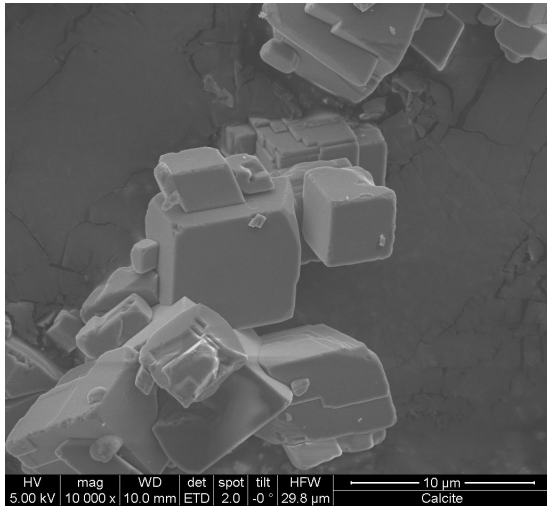
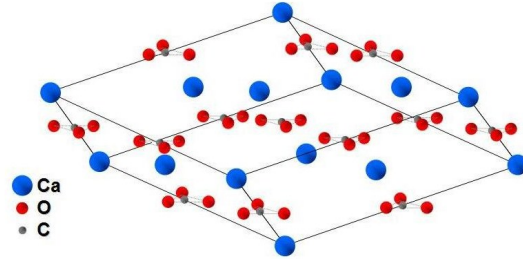


Figure 4.2: FTIR spectrum of calcite with the corresponding band list. The band assignment was taken from White1974



(a) SEM image of calcite with 10.000x magnification



(b) Calcite structure of $CaCO_3$

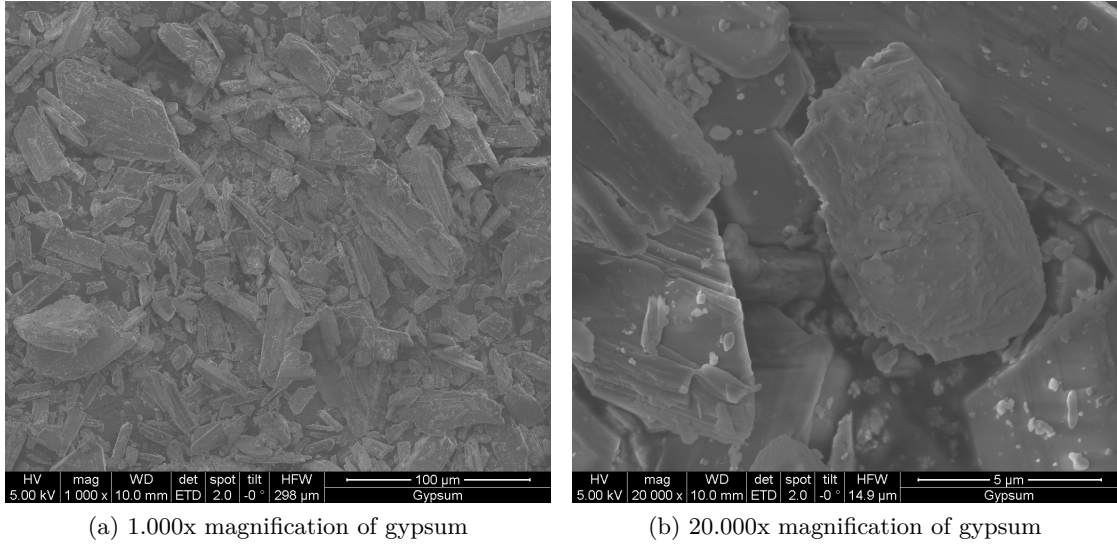
Figure 4.3: The calcite sample has cubic shaped crystals with an average grain size below $10\mu m$. The size distribution is quite narrow. The calcite structure has a rhombohedral lattice. The calcium atoms form a fcc lattice with carbonate groups located on the edges and in the center.

For the ice nucleation experiment a technical calcite from Sigma-Aldrich® was used. XRD and FTIR analysis showed no other adsorbates or mineral phases in the sample. The grains were cube shaped (fig.: 4.3). Calcite was an inactive IN. Furthermore a natural limestone was sampled at Hochtor, Gesäuse, Austria. XRD analysis was performed to get the mineral composition. The sample contains more than 99% calcite and showed similar ice nucleation behavior.

4.1.2 Gypsum

Gypsum is a calcium-sulfate with the chemical formula $CaSO_4 \cdot 2H_2O$. Natural occurring minerals crystallize monoclinic and incorporate around two water molecules into the crystal structure. Gypsum has a tendency to form needles (see fig.: 4.4). The gypsum sample was also studied by powder-XRD and FTIR. The XRD revealed that the sample is not pure. Some of the gypsum has lost its crystal water. The phase can be assigned as bassanite. On the gypsum grains no organics were adsorbed as can be seen in the FTIR (fig.:

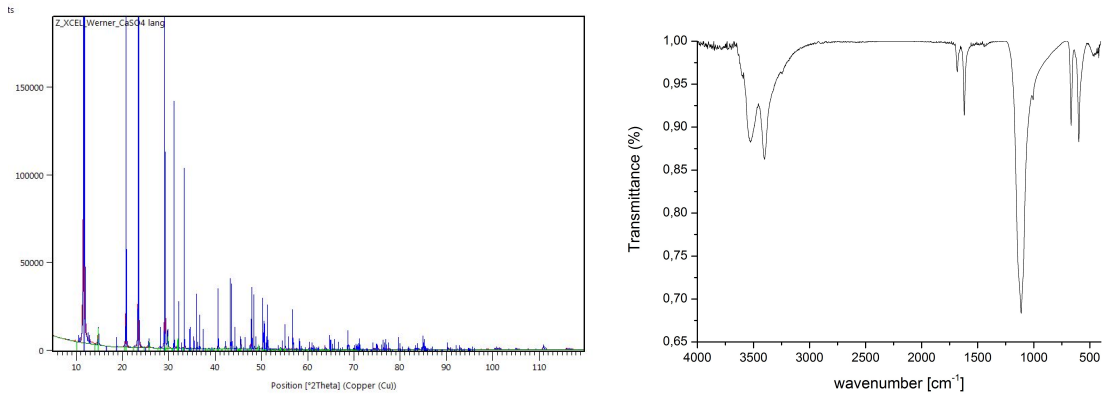
The gypsum sample can be considered as clean for our measurements. The in water depleted calcium sulfate is present in concentrations too low to inhibit nucleation on the normal gypsum grains. The water depleted gypsum phase was not active in the ice nucleation process as no specific initial freezing temperature was found. The initial freezing temperature for the gypsum sample was at $243K$ with a median freezing temperature of $239 \pm 1K$. Gypsum is not a good IN in the immersion freezing mode.



(a) 1.000x magnification of gypsum

(b) 20.000x magnification of gypsum

Figure 4.4: SEM images of the gypsum sample show the typical needles of Gypsum. Most grains have a length around $10\mu\text{m}$.



(a) XRD of gypsum sample, the data base peaks for gypsum are green and gray for $\text{CaSO}_4 \cdot 0.5\text{H}_2\text{O}$. The comment based on Haas et al. [14] position is 96% gypsum.

Figure 4.5: FTIR and XRD of the gypsum.

4.2 Silicate materials

A large difference in the ice nucleation activity of mineral dust, respectively for the silicates, was found in the experiments. Microcline, one quartz sample, kaolinite and ATD were active around $249 \pm 2K$, while all the others have median freezing temperatures well below $243K$.

4.2.1 Quartz

For the immersion freezing three α -quartz samples were used. This was chosen to exclude ice nucleation activity caused by potential impurities, which are quite common in natural occurring quartz. Foreign ions like Al^{3+} , Ti^{4+} , Fe^{3+} , Na^+ , K^+ may form active sites on the quartz surface. The used samples from Sigma-Aldrich[®], Fluka[®] and natural quartz were studied with ATR-FTIR and XRD. No surface adsorbates could be identified using FTIR. The bands in the FTIR-spectrum are as follows [11, 36]:

$1164cm^{-1}$ (E) and $1065cm^{-1}$ (E) are the Si-O stretching modes

$1071cm^{-1}$ (A_2) and $779cm^{-1}$ (A_2) are also Si-O stretching modes

$797cm^{-1}$ (E) and $696cm^{-1}$ (E) are Si-O stretching modes

$520cm^{-1}$ (E), $460cm^{-1}$ (E), and $495cm^{-1}$ (A_2) are the O-Si-O bending modes.

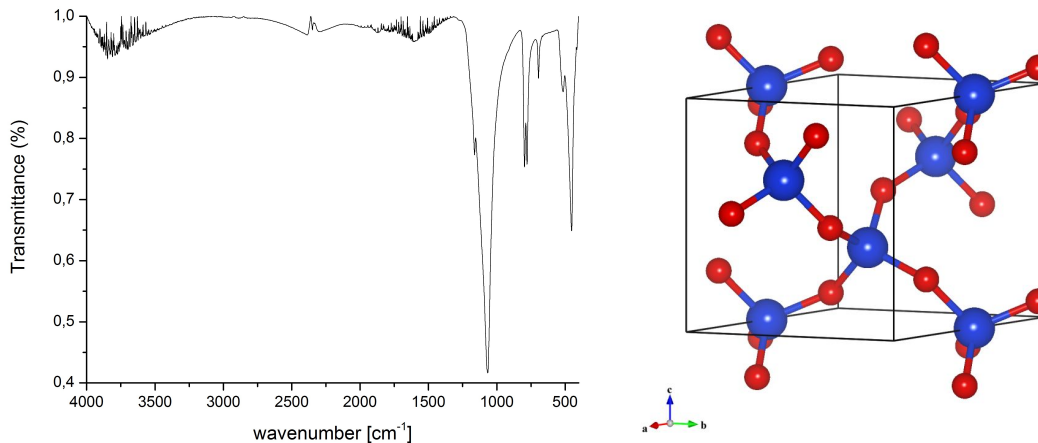
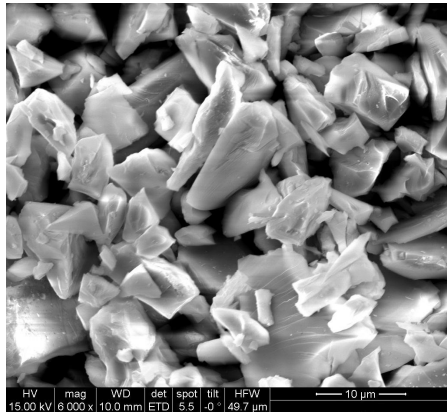
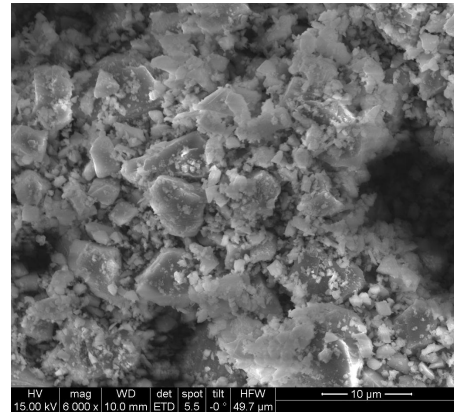


Figure 4.6: FTIR spectrum and structure of quartz. Peak identification was based on Ocaña [36]

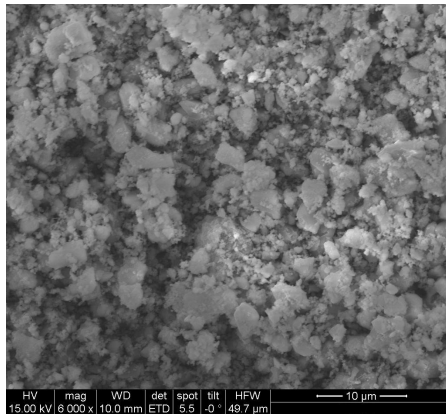
The powder diffractograms show all three samples to be pure α -quartz. The α -quartz unit cell is shown in figure 4.6. The substances were used in the immersion freezing experiment as purchased. The grain sizes of the three samples were different (fig.: 4.7). The natural quartz grains had a quite crystalline appearance with a grain size up to $15\mu m$. The size distribution is narrow with only a few grains smaller than $2\mu m$. The sample is pure quartz given by the EDX analysis. The two commercial samples, Sigma Aldrich[®] and Fluka[®] quartz are much smaller in size (BET-surface area: $5, 5 - 2m^2/g$). The grains have edges with more rounded shape. The sample might



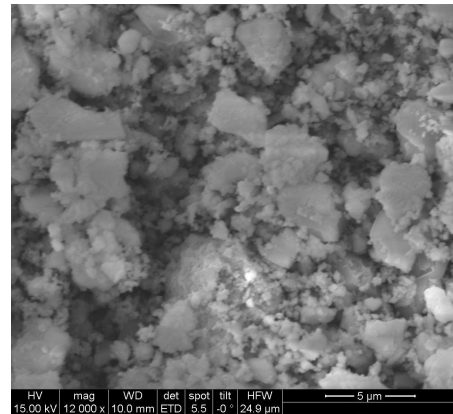
(a) SEM image of natural quartz



(b) SEM image of the Fluka quartz



(c) Sigma Aldrich quartz sample

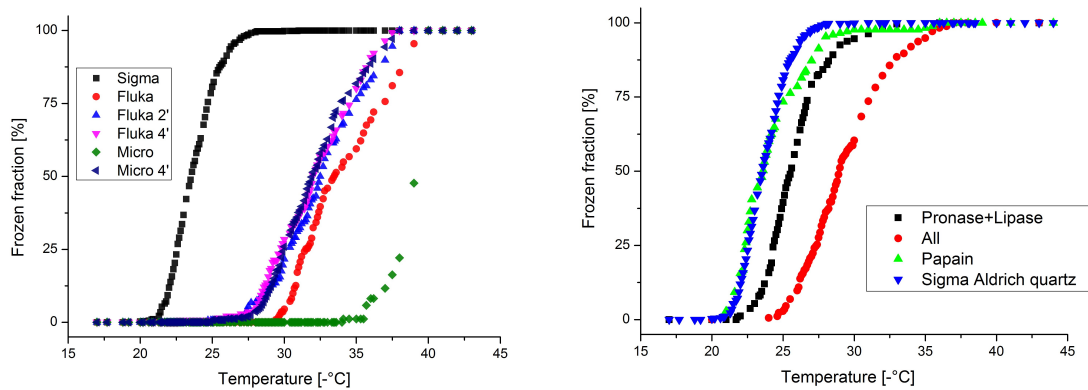


(d) Sigma Aldrich quartz 12.000x

Figure 4.7: SEM images of the different quartz samples. Images a,b,c were recorded with a magnification of 6.000x.

contain very small amounts of aluminum, potassium and sodium, but the value obtained in long term EDX measurements are within the uncertainty of the method. Both samples can be considered as clean α -quartz. The sigma Aldrich quartz contained the largest fraction of very small particles well below $1\mu m$. The median freezing temperature for the most active quartz sample (Sigma-Aldrich[®]) in the immersion freezing experiment is at $249 \pm 1K / -24 \pm 1^\circ C$. While the other two quartz samples are rather poor IN with median freezing temperatures of 239 (Fluka[®]) and $235K$ respectively.

The Fluka[®] and the natural quartz were milled in a hard metal swing mill. The ice nucleation activity increased by milling. The freezing curves for all quartz samples are summarized in figure 4.8. The initial freezing temperature of Fluka[®] quartz changed from 243 to $246K$ and the median freezing temperature changed from $239K$ (unmilled) to $240K$ ($2min$ milling) to $241K$ ($4min$ milling). The natural quartz was only milled



(a) Freezing curves for the different quartz samples (b) Freezing curves for enzyme treated quartz.

Figure 4.8: Freezing curves for differently processed quartz samples. The three different samples in the natural and milled state are shown on the left. On the right the freezing curves of the enzyme treated Sigma Aldrich[®] quartz are shown.

for 4min. Its nucleation activity was almost the same as for the Fluka[®] quartz after the same milling time with a initial around 246K and a median of 241K.

Further the Sigma-Aldrich[®] quartz was heat treated before the freezing experiment. The particles were heated for 4h at 523 or 773K. There was almost no change in the ice nucleation activity for the studied quartz. The Sigma-Aldrich[®] quartz was also suspended in water for a day. The produced quartz washing water had a few drops freezing at higher temperatures than homogeneous level. Around 20% froze above 237K.

An enzymatic treatment was also applied. A clear loss on activity could be seen with different enzymes added. The freezing curves are plotted in figure 4.8. Papain has almost no effect on the activity, while Lipase and Pronase E seem to be able to block active sites on the quartz surface. In addition, when all enzymes together were added the activity decreased further. Enzymes seem to be able to block active sites on the quartz surface. In addition when all enzymes together are added the activity decreases further. Nevertheless, the Sigma-Aldrich[®] quartz sample was still more active than the other two quartz samples when enzymes were added.

4.2.2 Feldspars

Three different feldspar samples were studied. Those were albite, microcline and andesine. XRD and FTIR were carried out on all three samples. SEM images were recorded, but only on microcline and albite EDX analysis was performed. The three feldspars showed different behavior in the ice nucleation experiment. While microcline had a median freezing temperature of $249 \pm 1K$, the others had median freezing temperatures below $243K$.

Microcline

The used microcline sample is a mixture of K-feldspar in the microcline phase and a mixed potassium-sodium feldspar. An exact quantification using XRD phase analysis was not possible. The total microcline content is around 60 – 80%. Despite the different feldspar phases no other impurities in the sample were found using XRD. The FEG-SEM images of the microcline sample are shown in figure 4.9. Averaged EDX measurements revealed a sodium:potassium ratio of around 1:3. The different grains varied in composition reaching from pure potassium-feldspar to almost 1:1 ratio of Sodium:Potassium. Single grains contained small amounts of calcium and iron. The grain size of the microcline sample was in the order of 1 – $20\mu m$ with a few grains reaching up to $50\mu m$.

TEM images of the microcline sample were recorded at the USTEM. The studied grains of the sample were crystalline. No surface dislocations or other features which might lead to an ice nucleation activity were found. The EDX data of the SEM experiment was confirmed. Two grains contained tiny amounts of iron, located at a certain site on the surface. Another grain had small calcium and magnesium contents. However,

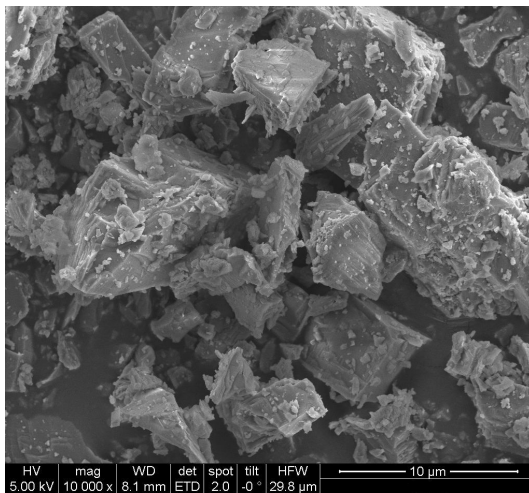
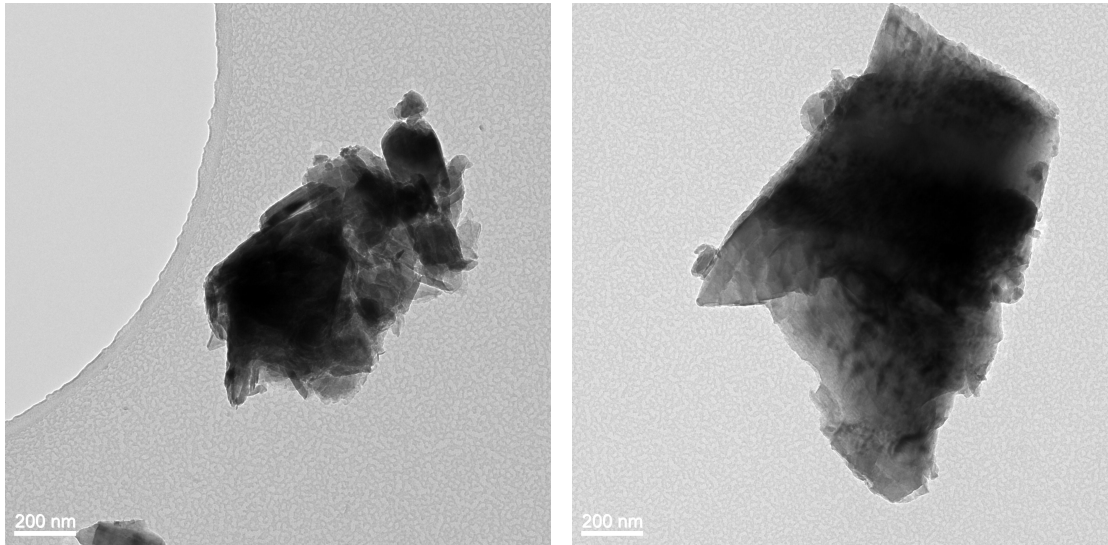


Figure 4.9: SEM image of microcline with a 10.000x magnification. Some grains are up to $50\mu m$ in size, those are not visible in this image.

<i>Element</i>	<i>Wt%</i>	<i>At%</i>
O	43,5	58,6
Na	2,0	1,9
Mg	0,3	0,3
Al	10,9	8,7
Si	32,0	24,5
K	10,2	5,6
Ca	0,0	0,0
Fe	0,9	0,4

Table 4.1: Composition of the microcline given by EDX in the SEM using the K_{α} lines. The size of the sampling site was $70 \times 60 \mu m$



(a) TEM image of a K-feldspar containing magnesium

(b) TEM image of a pure crystalline K-feldspar

Figure 4.10: TEM images of microcline. EDX measurements were also performed on these grains. The grain shown on the left contained magnesium. The one to the right is a pure K-feldspar.

these impurities were only found in minor quantities. Most grains are just pure microcline or microcline with some sodium content. The surface of the grains is rather smooth and flat. The microcline sample had also been milled to smaller grain sizes for better TEM resolution. No other features on this sample were found. The sample was crystalline, but amorphizes in the electron beam.

The median freezing temperature of crushed and freshly milled microcline varied between 251 ± 1 and 249 ± 1 depending on the used batch. The transition was always sharp. The highest median freezing temperature was found for the fine milled sample. All three samples were exposed to heat treatment. The relative change in median freezing temperature was almost the same for all samples with aT_{50} of $250 \pm 1 - 247 \pm 1$. The values differ over a range of $4K$ between all the temperature measurements and different samples. All freezing curves are single step and more than 90% of the drops in the $20mg/ml$ samples froze heterogeneously. The freezing curve of the fine milled microcline is shifted to higher temperatures.

Microcline samples were enzymatically treated. Lipase¹ and Pronase E shifted the freezing curves to lower temperatures with median freezing temperatures around $243K$. The curves are slightly broadened. In the Papain treated microcline sample only 30% of the droplets froze around $243K$, the rest froze homogeneously. Onozuka has only a minor effect on the freezing behavior of microcline by shifting the curve by $1K$ to lower temperature which is within measurement uncertainty. All enzymes together lead

¹The different enzymes are explained in section 2.3

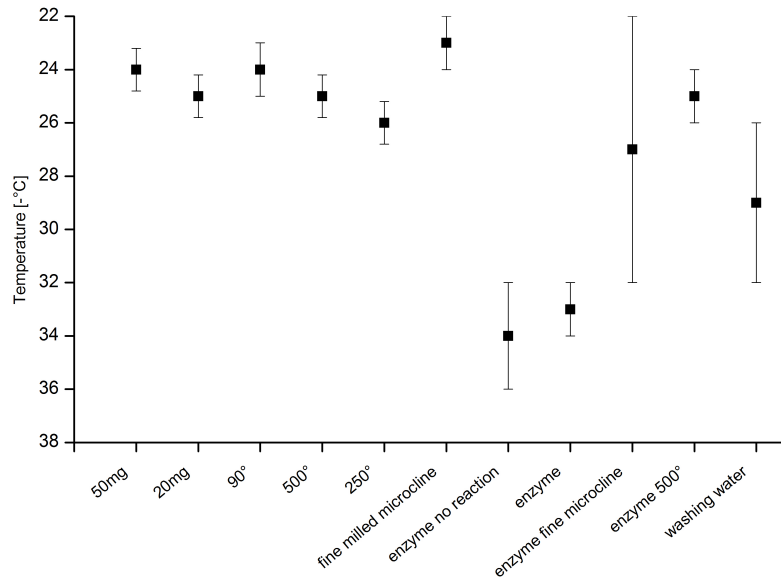


Figure 4.11: Median freezing temperatures for differently treated microcline samples. The samples are from left to right: 50mg/ml and 20mg/ml particles, 20mg/ml of 90/250/500° preheated particles, finer milled microcline particles, enzymes mixed with the particles which were measured before the enzymes could react chemically, classical enzyme treated microcline, and fine milled microcline, enzymes reacted first with the particles which were than heat treated at 500° and microcline washing water. The non enzyme treated samples have all median freezing temperatures of $249 \pm 1, 5K$. Median freezing temperatures are the same for 4h enzyme treated and enzyme mixed microcline. The median freezing temperature after enzymatic treatment and heat treatment is the same as before any treatment.

to a broad curve with a median freezing temperature of $241 \pm 1K$. If the enzymes were added to the microcline suspension and the suspension was measured right away in the immersion freezing experiment without any possible reaction time the results were the same. To the fine milled microcline only the enzymatic cocktail was added. The resulting freezing curve was a two step curve with 50% of the drops freezing at the freezing temperature of pure microcline and the rest freezing close to and at homogeneous freezing temperature. If the enzymatic treated samples were exposed to a heat treatment the original nucleation activity of microcline could be regained. The activity of the finer milled particles decreased slightly, but was still within measurement uncertainty. The whole enzyme-heat treatment process is reversible. Only in the initial step of the fine milled microcline a slight loss of activity was observed.

The washing water of microcline did freeze above the homogeneous freezing temperature. The freezing curves for the normal microcline washing water had a step like appearance (fig. 4.12). With 50% freezing above $245K$, but 20% freezing homogeneously. The washing water produced from the fine milled microcline particles is more active than the washing water of more coarse microcline particles. The median freezing temperature

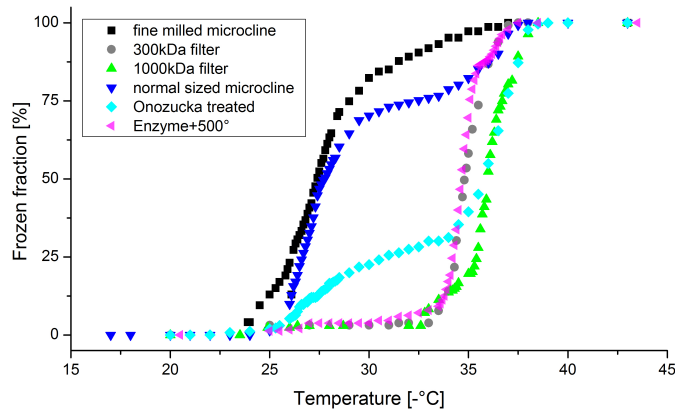


Figure 4.12: The freezing curves for the differently treated washing waters. The black curve is the washing water of the fine milled microcline, gray and green are filtered samples of this washing water. Blue is the washing water of the normal sized microcline particles, which was treated with onozuka (cyan). The particles were also enzyme treated and heated before a washing water was made (magenta).

is around $1K$ higher while less drops freeze homogeneously. The washing water was filtered with different size exclusion filters. Neither the $1.000kDa$ nor the $300kDa$ filtered water was active in the ice nucleation experiment. If enzymes were added to the washing water the ice nucleation activity was almost gone. Only for onozuka around 25% of the drops still froze as before the treatment. SEM revealed that the washing water contained tiny microcline particles. The particles were of sizes up to $500nm$ and much smaller. An exact analysis of the particles seen is lacking, but they look like feldspar. However, the ice nucleation of the washing water of temperature treated particles was much lower.

Albite

The albite sample is considered as low-albite, which is the more ordered phase of albite. In the XRD only the low-albite phase was found. SEM-EDX analysis revealed small amounts of potassium and calcium. The average particle size is around $1 - 20\mu m$, and therefore almost the same as for microcline. On the surface of the albite sample no molecules are adsorbed. The bands in the FTIR (fig. 4.13) are Si-O stretching vibrations at 1136 and $1100cm^{-1}$, the next two around $1000cm^{-1}$ are the Si(Al)-O stretching frequencies. The bands between 700 and $800cm^{-1}$ are the Si-Si and Si-Al stretching modes, the next bands are at $642cm^{-1}$ the O-Si(Al)-O bending, at $587cm^{-1}$ the O-Si(Al)-O bending, $542cm^{-1}$ and $460cm^{-1}$ are asymmetric and symmetric O-Si-O bending modes coupling with the Na-O stretching mode [15]. The last visible band in the spectrum is the Si-O-Si deformation. The noise in the spectrum is atmospheric CO_2 and water, which can be recognized due to their vibrational fine spectra.

TEM images of the albite sample are shown in figure 4.14. The albite sample is crystalline and on the particles used in the immersion freezing experiment no surface features were visible. The EDX measurement on different grains revealed certain impurities. On around 30% of the grains small lead containing areas were found. These were circular shaped. A bit of molybdenum was also present in the sample. EDX mapping over a crack on two particles were performed. There was no depleting or accumulation of certain elements within the crack. A single hard metal grain was found which is a result of the crushing process.

The median freezing temperatures for albite are $239 \pm 1K$ for $20mg/ml$ and $240 \pm 1K$ for $50mg/ml$. The $773K$ heat treated albite particles did have almost the same freezing behavior as before heat treatment. The albite sample was grained to lower particles size using a ball mill, but exact particle size measurement is lacking. After grinding the initial freezing behavior changed. Onset freezing was around $249K$. This feature was gone after heat treatment. The process was reproducible, but the curves of the fine powder did not look exactly the same. Enzymatic treatment was only done with Papain which did not show any effect.

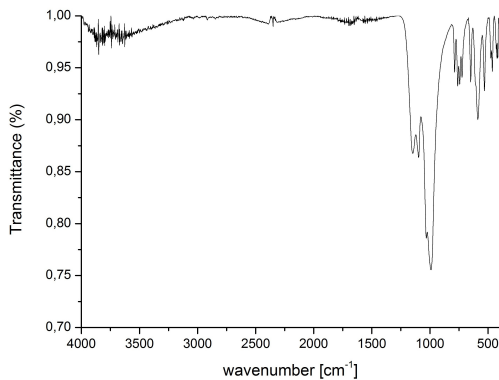
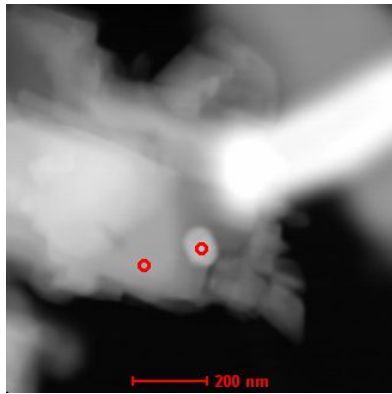


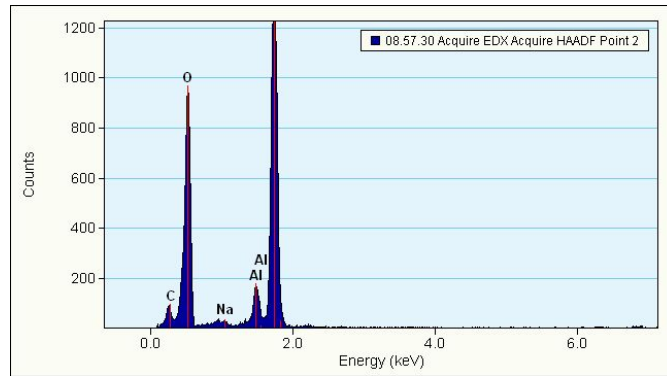
Figure 4.13: FTIR spectrum for albite

ν [cm^{-1}]	Mode
1136, 1094	Si-O stretching
1017, 996	Si(Al)-O stretching
792, 763	Si-Si stretching
743, 720	Si(Al)-Si stretching
642, 587	O-Si-O bending
542, 460	O-Si-O bending coupled with Na-O stretching
428	Si-O-Si deformation

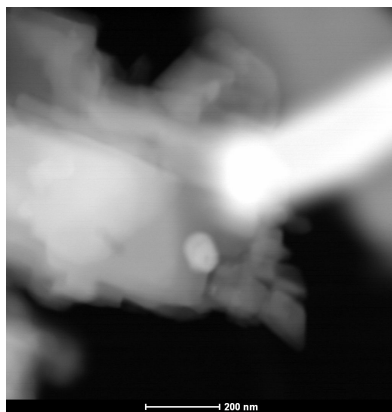
Table 4.2: Corresponding peak list for albite



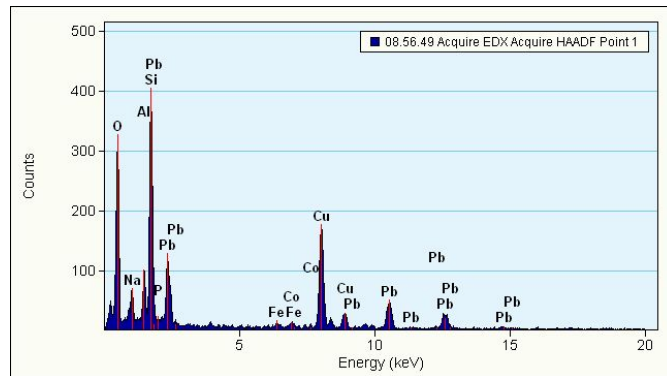
(a) EDX measuring spots



(b) EDX of the left spot. This is the Albite matrix.



(c) SEM image of the particle



(d) EDX of the right bright dot. It is a lead impurity

Figure 4.14: Images of an albite particle with the lead impurities. These are well localized at circular shaped areas. The total lead concentration within the sample is low, but this feature was found on more particles. The copper and carbon peaks in the EDX spectra are from the substrate.

pH dependance measurement

As the exchange of oxygen-hydrogen species is highly pH depended immersion freezing experiments under different pH conditions were performed. Therefore albite and microcline particles were suspended in a $10^{-5} \text{ mol/l HCl}$ and a $10^{-5} \text{ mol/l NaOH/KOH}$ solution. The solutions had a reaction time of 48h before the immersion freezing experiment was performed. The freezing results at pH 5 and 9 were the same as at pH 7. Slight pH changes did not show any influence on the ice nucleation behavior of feldspars.

Andesine

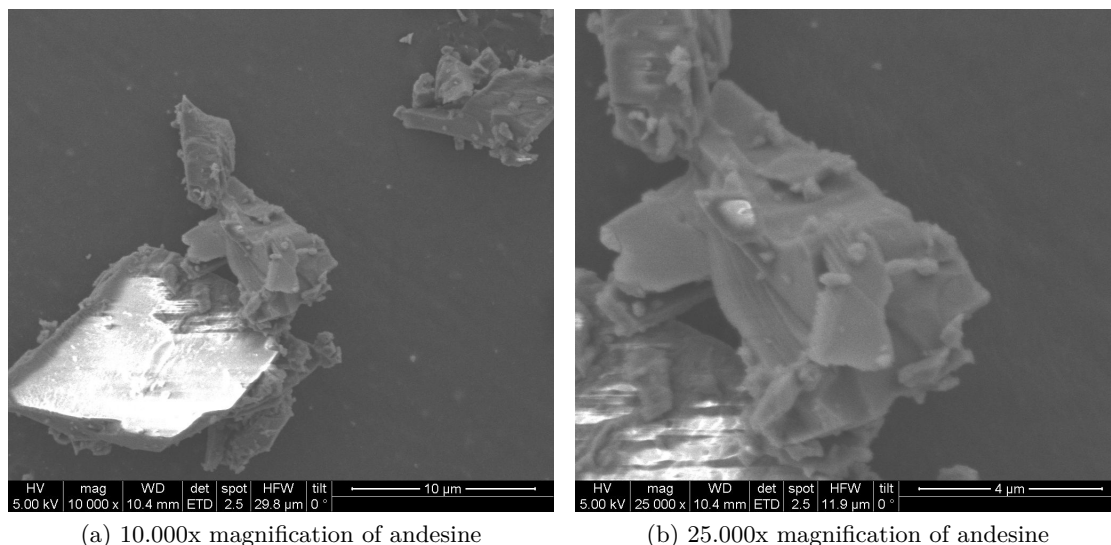
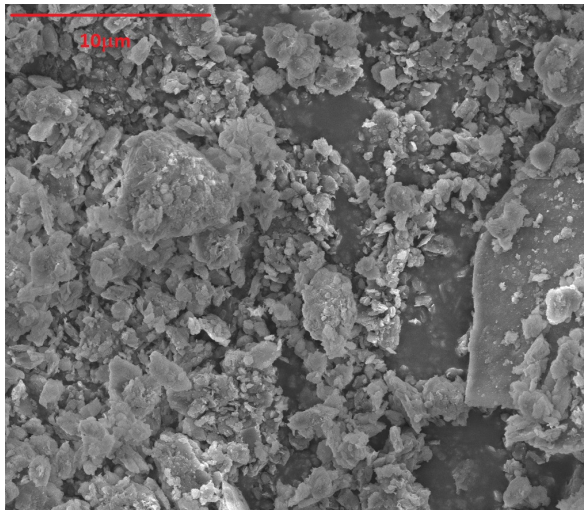


Figure 4.15: SEM images of andesine with different magnifications of the same grain. The white area is an experimental artifact of surface charging.

The andesine sample has a Ca:Na ratio of 50:50. In the XRD only the andesine phase with around 50:50 Na:Ca was identified. The FTIR spectrum is a clean andesine spectrum with no additional bands despite the CO_2 , H_2O noise. The freezing behavior for the andesine is almost the same as for albite with a median freezing temperature of $240 \pm 1K$. The initial freezing temperature was $244K$. The particle size observed in the SEM is well below $20\mu m$ (fig. 4.15). The grains have the same appearance as the other feldspars. EDX data for this sample was not recorded.

4.2.3 Montmorillonite

Montmorillonite is a clay mineral. It is able to nucleate ice up to temperatures of $246K/-27^\circ C$. The median freezing temperature is at $240 \pm 1K/-33^\circ C$. The freezing curve for montmorillonite is quite broad. The powder diffractogram is shown in figure 4.17. The used montmorillonite sample contains measurable amounts of other minerals: quartz and muscovite. The montmorillonite samples was purchased milled from Sigma-Aldrich[®]. The grains varied in size given by the SEM images (fig. 4.16). The elemental composition is given in table 4.3. The used montmorillonite contains around 1% iron, which is more than the average montmorillonite.



<i>Element</i>	<i>Wt%</i>	<i>At%</i>
OK	47,36	61,81
NaK	0,33	0,3
MgK	1,31	1,13
AlK	8,64	6,68
SiK	37,78	28,09
KK	0,122	0,65
CaK	0,3	0,16
TiK	0,53	0,23
FeK	2,51	0,94

Figure 4.16: SEM image of Montmorillonite with a 10.000x magnification.

Table 4.3: Composition of the montmorillonite given by EDX in the SEM using the K_{α} lines.

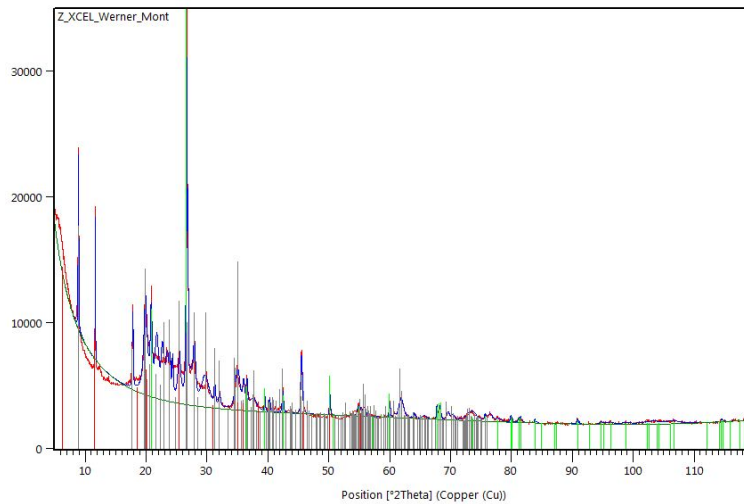


Figure 4.17: Diffractogram of the montmorillonite sample with peak matching using the pdf database. The sample contains mainly α -quartz(gray), muscovite (red), and montmorillonite (gray). A quantification was not possible.

4.2.4 Kaolinite

Kaolinite is the direct weathering product of feldspar. The kaolinite sample is an active ice nucleus. The median freezing temperature is $248 \pm 1K / -25^{\circ}C$. The shape of the freezing curve did not react on heating. An increased concentration of kaolinite particles in the suspension led to an agglomeration. These kaolinite domains bind some water around them. Therefore non circular water areas could be seen during the cryo-microscopic measurement (fig. 4.18). As expected, these large domains froze at higher temperatures than the small drops. This leads to drastically increased initial freezing time. Kaolinite was the only sample showing this behavior for a concentration of $50mg/ml$. The kaolinite sample contained 5 – 10% quartz, halloysite, and muscovite. The particle size distribution for kaolinite was quite large. Grains of around $5 - 10\mu m$ and also very small grains below $1\mu m$ were present at higher quantities.

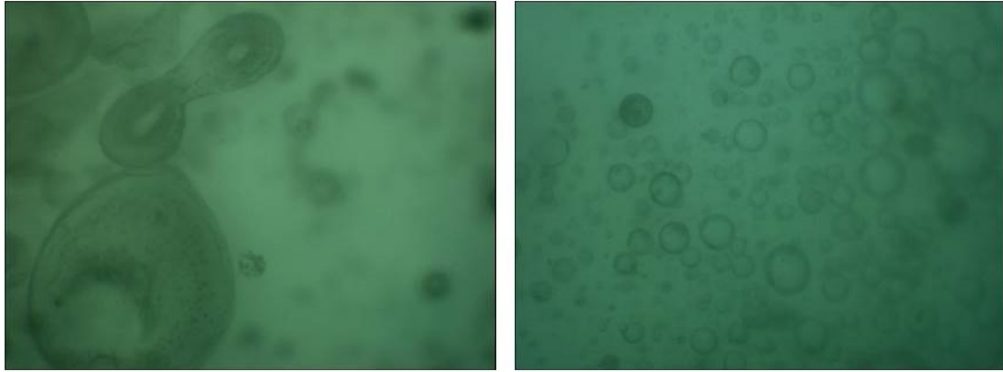


Figure 4.18: Images of the oil/water suspension drop under the cryo-microscope. The left image is from the $50mg/ml$ kaolinite suspension. The right one from the $20mg/ml$ suspension.

4.2.5 ATD

Arizona test dust is a natural dust from Arizona. It is manufactured by PTI- powder technology inc. The composition of the natural sample was studied using SEM - EDX and XRD. The dust is mainly composed of quartz. The FTIR spectrum is mainly a quartz like spectrum, showing also some feldspar bands in the region of $500 - 700\text{cm}^{-1}$. There is a broad band around 1430cm^{-1} which can be attributed to calcite. Around 870cm^{-1} a small band of the out of plane bending of the carbonate group is visible. In the EDX small amounts of calcium were found too, indicating some calcite content of the sample. The EDX representing oxide composition is given in table 4.4. Most SiO_2 is present as quartz, the rest are mainly different feldspars. Feldspars account for 30 – 50% per mass of the ATD sample using the EDX data. An exact quantification using classical powder XRD was not possible, but estimations are 15 – 20% microcline, 15 – 20% sodian andesine and 5 – 10% of other feldspars. The ATD sample had a particle size of $1 - 10\mu\text{m}$ (fig. 4.19). The particle size distribution is narrow and the shape of the particles is quite similar. The manufactured dust is also filtered so very small particles are not present in the sample. The sample was used without further milling in the ice nucleation experiment. ATD was as active as microcline and the Sigma Aldrich[®] quartz sample with a median freezing temperature of $250 \pm 1\text{K}$. The ATD sample was also heat treated before the measurement. The freezing curve shifted a bit to lower temperatures and got a bit broader. While the initial freezing time stays almost constant the gradient decreases. The behavior is reproducible but still within the uncertainty of the experiment.

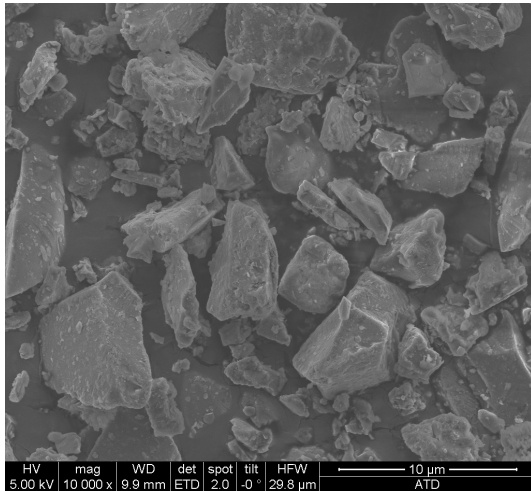


Figure 4.19: SEM image of ATD with a 10.000x magnification.

<i>Oxide</i>	<i>At%</i>	<i>Wt%</i>
Na_2O	2,3	2,2
K_2O	1,5	2,2
MgO	2,0	1,2
CaO	2,3	2,0
SiO_2	85,9	82,0
Fe_2O_3	1,1	2,6
Al_2O_3	5,0	7,9

Table 4.4: Composition of the ATD sample given as oxides in %.

4.2.6 Volcanic Ash

The volcanic ash sample is from Iceland. The purchased powder had a grain size distribution of $500nm - 500\mu m$. The sample was first hand milled. The hand milled sample was studied with XRD and FTIR. All bands in the IR were quite broad and overlapped. An exact identification of the bands was not possible. The main features are the typical silicate bands. There is high evidence that no organics are adsorbed. The volcanic ashes main component is albite, with many others minerals present. Quantification of the minerals was not possible with XRD. Feldspars, quartz and iron-titanium oxide were found at higher quantities. The hand milled ash was first used in the ice nucleation experiment. A concentration of $20mg/ml$ was used. As some grains were larger even after hand milling with the agate mortar they sedimented from the suspension. A first measurement was performed. The hand milled volcanic ash sample had a median freezing of about 241 ± 3 . The freezing sets in around $246K$ and continues up to lower temperatures. A milling with a steel-ball-mill was done to reduce the particle size of the large grains. The freezing curve did change only slightly. This milling process was not complete as some minerals were too hard. The freezing curve shows an initial freezing similar to the hand milled sample, but most drops freeze homogeneously. A change in the representative composition of the suspended particles can't be excluded. Even though it might not represent the true nature as the hard component may only occur in particle sizes with an atmospheric aerosol lifetime too small. The ash was milled in a hard metal swing mill to get all minerals to sizes below $10\mu m$. The hard component, which could not be milled with the agate and a steel ball mill, was expected to be some silicon-aluminum oxide. After the milling process, the onset freezing was almost constant but only a few drops froze well above homogeneous freezing temperature. The milling was performed for $8min$ resulting in a reduced grain size for all particles well below $1\mu m$.

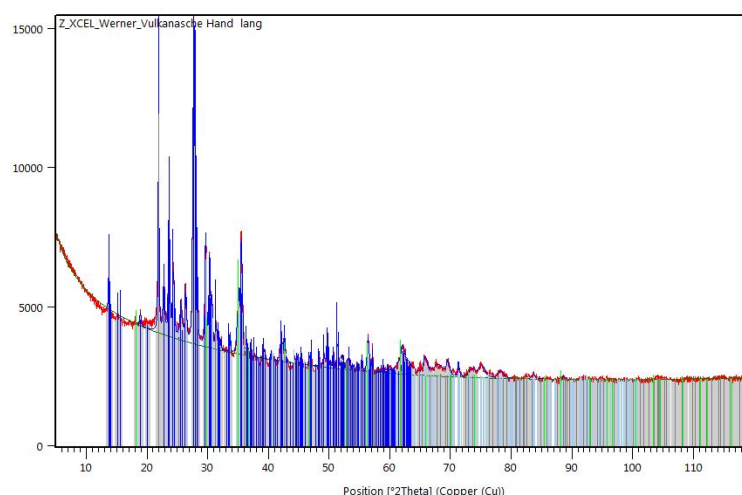
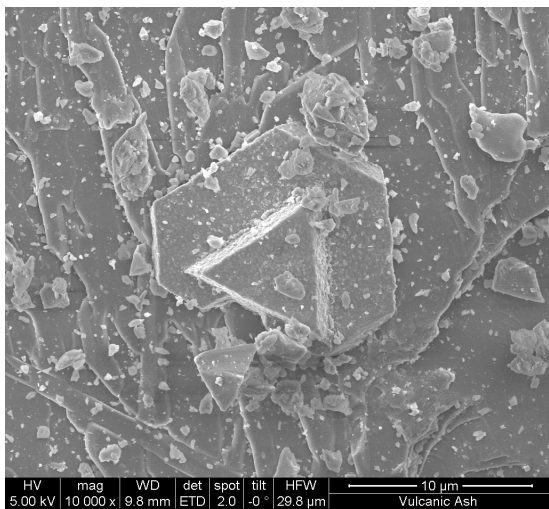
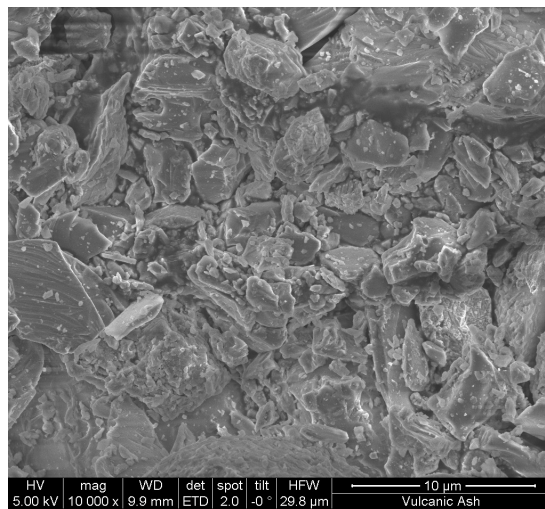


Figure 4.20: Diffractogram of volcanic ash with albite, quartz and iron-titanate for peak fitting.



(a) Iron-titanium oxide particle in the volcanic ash sample. This is the only hexagonal $(Fe, Ti)O_3$ which was found in the SEM. Powder XRD estimates the phase around 5 – 10%.



(b) The bulk of the volcanic ash is mainly composed of albite and other sodian feldspars. The crystallinity is lower than in the feldspar samples.

Figure 4.21: SEM images of the volcanic ash sample with a 10,000x magnification. These images were taken after the ash was hand milled.

Discussion

The ice nucleation activity of the investigated minerals is quite different (fig. 4.1). Median freezing temperatures range from $250K$ to $236K$. Only four samples are active at temperatures above $243K$. These are kaolinite, Sigma Aldrich[®] quartz, microcline and ATD. All these materials are silicates, but only two other none silicates were studied. The silicates are the most abundant mineral dusts, but most are not active IN above $243K$. It is still not possible to describe the heterogeneous nucleation process on a molecular level on mineral dust particles exactly.

Ice nucleation on mineral dust particles happens at nucleation sites on the surface. Every nucleation site has a certain temperature at which it becomes active (compare the singular model in section 1.2.2). A single mineral may contain many different sites. It is not possible to study the sites directly, but some conclusions can be taken from the immersion freezing experiments carried out in this study. Active sites are only found in the silicates. Klier et al. had suggested that silanol groups play an important role in the ice nucleation process [22]. However, the silanol groups as functional groups alone do not act as a good IN as they are present in almost all silicates in aqueous solution. It is rather a complex interplay between the ice and local surface structure of the mineral particle and therefore the arrangement of the functional groups. The local electronic configuration and distance and arrangement of functional groups influence the capability of acting as a good IN. The flexibility of surface groups like hydroxyl groups as well as the size match between the surface and the ice structure is important (compare Hu et al. [19]). A molecular site is defined as an arrangement of functional groups able to stabilize ice on the surface in this work, as indicated in the figure 5.1 atomic scheme on the right. The molecular site is thought to be only a few atoms in size. Molecular sites can be close together on the surface. Ice is stabilized at these molecular sites and, if the distance is low enough, also between them. The molecular sites form a domain (see gray areas in figure 5.1) on the surface where water in an ice-like structure is stabilized. These domains are the nucleation sites and if the stabilized ice cluster is almost as large as the critical ice cluster needed at the given temperature for ice nucleation the site is an active

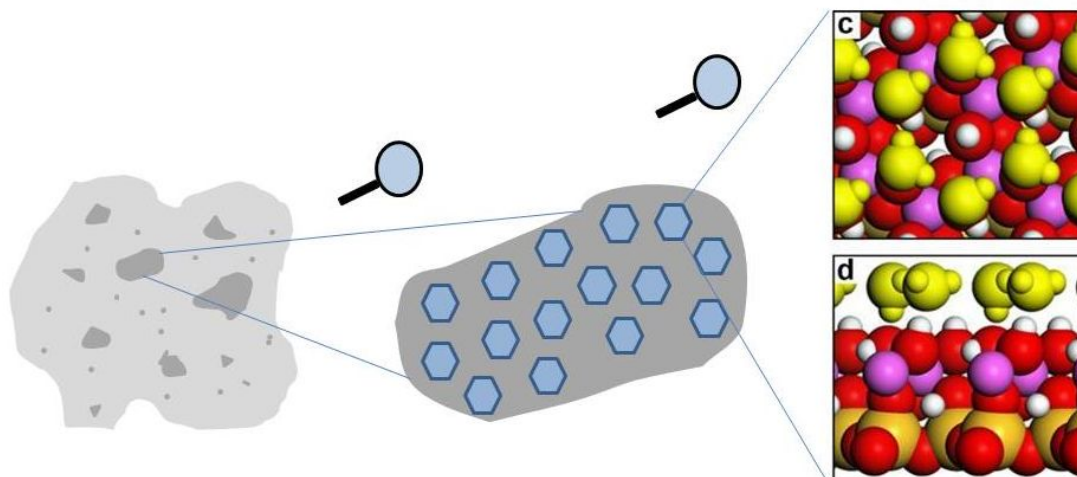


Figure 5.1: Schematic description of active sites on mineral dust particles. Different nucleation sites (dark gray) are found on the dust particle (light gray). The nucleation sites are domains of molecular sites (indicated with blue hexagons) where water molecules are stabilized in an ice-like structure. The ice-like structure is stabilized via hydrogen bonds by a well fitting amphoteric part of the particle surface. Part of the image is taken from Hu et al. [19].

nucleation site at this temperature. The assumption of specific molecular sites is based on the fact that with only partial surface coverage with enzymes the ice nucleation activity is lowered. In addition, the activity can be increased by increasing the surface area. The ice nucleation activity in the investigated silicates is so to say not a property of a perfect surface. This could be shown by the enzymatic treatment and by the fact that the coarse quartz was not active (see fig. 4.8a). The nucleation process takes place at the specific sites, where an ice nucleus forms, which initiates ice formation in the whole drop. The size of the nucleation sites, and therefore, the nucleation temperature of the sites conforms to a specific distribution. The distribution is based material specific on the concentration of molecular sites. Molecular sites may also vary in stabilization energies of the ice-like arranged water molecules. The „soccerball“-approach by Niedermeier et al. can be used to describe the here discussed model. The particles have different nucleation sites which are active at different temperatures, but within the here presented description there is no direct conclusion why the size of the domains should be discontinuous leading to discrete nucleation sites and contact angles in a „soccerball“-description. The theoretical models of stochastic and singular freezing are not as suitable here. Time dependence was not considered as the freezing experiments showed almost no time dependance.

Molecular sites are more or less common on different minerals. The different concentrations of the molecular sites lead to different distribution of nucleation site sizes in the different studied samples due to their structural and chemical difference. Molecular sites have a certain geometry/arrangement of the atoms and $Si - O$, $Si - OH$, $Al - O$, $Al - OH$ surface groups have a certain flexibility. The functional groups important for

ice nucleation are either hydrogen bond donors or acceptors, like hydroxyl, oxygen, oxide or fluorine groups (compare Shen et al., and Hu et al. [19,45]).

The tectosilicates, quartz and feldspar, seem to be the most promising candidates to study the difference as close related structures have different nucleation behavior and therefore active site densities. In addition the largest difference in ice nucleation temperature was found within this group. Feldspars seem to have more active sites at higher temperatures, meaning that the feldspar surface can stabilize larger ice clusters. This means feldspar has more molecular sites than quartz where water molecules in ice-like arrangement are stabilized and those may be close to other molecular sites. The reason might be the influence of the different composition of the minerals leading to distortions and defects on the surface. The feldspar surface is more prone to have ionic surface sites than quartz. Nevertheless, as sodium and calcium containing feldspars have lower freezing temperatures as potassium feldspar the „process of ice nucleation“ is much more complex. Other atoms than the hydroxylated silicon or aluminum atoms at the surface of the particles may also influence the nucleation process. Klier et al. had described the influence of fluorine in micas before [45]. In the next section the ice nucleation activity of the different studied samples is discussed.

5.1 Ice nucleation of the different dust particles

5.1.1 Calcite

Calcite is not a good IN with a median freezing temperature below $238K$ (see figure 4.1). The nucleation temperatures are only slightly above homogeneous level. The surface of calcite in humid air and liquid water adsorbs water molecules. The particles may be covered with layers of water [26,27]. The water binds either to a calcium or via hydrogen bonds to a surface oxygen atom. This interaction is quite strong. The water molecules are tightly bond and are well located in their positions on the surface. The distance between single water molecules does not match the distances in the ice structure. The calcite surface is therefore not able to stabilize larger ice clusters. Jimenez et al. suggest that some calcium ions are released after adsorption of water [51]. Calcium ions form a hydration shell, which also may not favor ice formation as the calcium ion has a stronger interaction with water than the water molecules among each other (see section 5.1.5 for a detailed description). The well adsorbed water molecules and these calcium ions inhibit any possible stabilization of water molecules in an ice like structure. The natural limestone sample behaves the same way. Therefore, calcite is not important for ice nucleation in the atmosphere.

5.1.2 Gypsum

Gypsum is a slightly better IN than calcite, but with a median freezing temperature of $239K$ its influence on cloud glaciation can be neglected. Gypsum may show similar

behavior as calcite in water. Heterogeneous nucleation could occur by binding to the crystal water if it is exposed to the surface. There is no evidence that the $CaSO_4$ is a better IN than calcite. The surface might bind water too strong in positions which do not favor ice cluster formation as for calcite. In addition, the adsorption process may release some calcium ions, which bind water too near to the surface. The calcium ions in the surface bilayer may also inhibit ice nucleus formation at potential active defect or impurity sites. The initial freezing temperature is below $244K$ so there are even no really good nucleation sites with low site density on gypsum.

5.1.3 Silicates

The difference in the ice nucleation activity of the silicates cannot be assigned to the crystallographic structure directly as quartz and microcline are tectosilicates, while kaolinite is a phyllosilicate [8]. There seems to be more than just a direct crystallographic and structural reason to determine the ice nucleation activity as even within the feldspars, which belong to the same mineral family, only the K-feldspar (microcline) was active (see section 4.2.2. They belong to the tectosilicates (quartz, feldspars) and the phyllosilicate group (Kaolinite, Montmorillonite). The base unit of all silicates is a SiO_4^{4-} tetrahedron. These tetrahedra may be connected via corner, edges, or faces forming multidimensional structures like rings, chains or 3D-networks. The tectosilicates have a 3D-network of corner connected tetrahedrons. Phyllosilicates consist of sheets. In most natural silicates some silicon atoms are replaced by aluminium atoms. The charge is compensated by other cations. All investigated materials except quartz belong to this aluminosilicate group. The base sheet or network structure is partly distorted by the cations.

5.1.4 Quartz

The thermodynamic stable α -quartz had different ice nucleation activities for all three studied samples. The Sigma Aldrich[®] quartz had a median freezing temperature of $249 \pm 1K$, Fluka[®] quartz became active below $244K$ and had median freezing temperature of $240 \pm 2K$ (figure 4.8a). Temperature treatment did show no effect on the Sigma Aldrich[®] quartz, therefore the increased activity of this sample is not a result of adsorbed organic or biological IN. The low resolution XRD-diffractograms of all three tested α -quartz look the same and no other phase was present. The active Sigma Aldrich[®] and Fluka[®] quartz may contain small amounts of aluminum, potassium and sodium given by the SEM-EDX analysis. The amounts are very low and may only be noise. The main difference in the ice nucleation activity of the three quartz samples is a result of the different particle size and the resulting surface area. The most active sample is the Sigma Aldrich[®] quartz with the smallest particles and therefore the highest surface area ($5, 5m^2/g$) and number of particles per droplet. The Fluka[®] quartz sample is a poor IN. The natural quartz is almost inactive. The activity was increased by milling the samples. Fluka[®] and natural quartz were almost as active after 4 minutes milling with the hard metal swing mill. Through the milling process the surface area of the sample is increased. Even though the Fluka[®] quartz has some very small grains, the milling process leads to almost the

same grain size as the milled natural quartz. The surface area of the initial quartz samples was measured by BET. In agreement with the SEM images (fig.: 4.7) the ice nucleation activity increases with surface area. The surface area of Sigma Aldrich[®] was $5,5m^2/g$, Fluka[®] quartz was $2m^2/g$, and $0,5m^2/g$ for the natural quartz samples as used in the initial freezing experiments. The activity of Sigma Aldrich quartz is not reached by milling for 4 minutes, but it is assumed that with a better milling equipment and a much longer milling time, the same activity for the other quartz samples could be achieved. As the Fluka[®] quartz, which was already active before milling, shows an increased activity with milling time further milling would lead to higher freezing temperatures. The initial freezing is clearly shifted to higher temperatures with milling (fig. 4.8a). This leads to the conclusion that the nucleation happens on specific nucleation sites, which may be created in higher number through milling processes. The milling process creates new functional groups by introducing more defects to the surface. In addition the surface area per drop is increased by milling as the same particle mass concentration was used in the experiment (see chapter 4). There are different sites which become active at a given temperature and have a certain site density. By increasing the surface area of the sample the amount of sites in a single drop increases. Obviously, quartz has good nucleation sites which are active at $250 \pm 2K$. The site density per surface area of those is quite low in natural and Fluka[®] quartz, so only in the Sigma Aldrich[®] quartz enough particle surface is available in every drop. In the unmilled other quartz samples no drops freeze in this temperature region. After the milling process some drops freeze above $248K$, but there number is low. Other sites on the quartz are more common, those are poor IN, active around $241 \pm 2K$. The quartz sample with medium surface area like the milled quartz samples and the Fluka[®] quartz show main freezing around this region. All ice nucleation active sites are too scarce to initiate nucleation in the case of coarse natural quartz with the lowest surface area. The ice nucleation on the quartz samples can't be fitted to the singular model as the n_s curves of the three sample do not fall into a line. The ice nucleation activity still increases with surface area, but mechanical milling and/or surface impurity atoms also have an influence as can be seen in figure 5.2. The three quartz samples are different in their ice nucleation activity and the active site density (n_s). Sigma Aldrich[®] quartz has the most defects and best nucleation activity, independent of the higher surface area.

The enzymatically treated Sigma Aldrich[®] quartz was a rather poor IN (see figure 4.8b). As the enzyme concentrations are too low to result in a colligative effect in the experiment a freezing point lowering can be neglected. Homogeneous freezing was therefore not influenced by the enzymes. The enzymes themselves do not nucleate ice. It is assumed that the different ice nucleating sites of quartz are blocked by the enzymes. While Papain is not able to block the very best sites, the other enzymes are able to block the sites active around $250 \pm 2K$. The drops freeze at lower temperatures, but still heterogeneous. For Pronase and Lipase the median freezing temperature shifts to $247 \pm 1K$. This supports the assumption of the existence of another site where an ice nucleus can form, which may still be less frequent than the sites which are active in the more coarse quartz samples. All enzymes together lower the freezing temperature

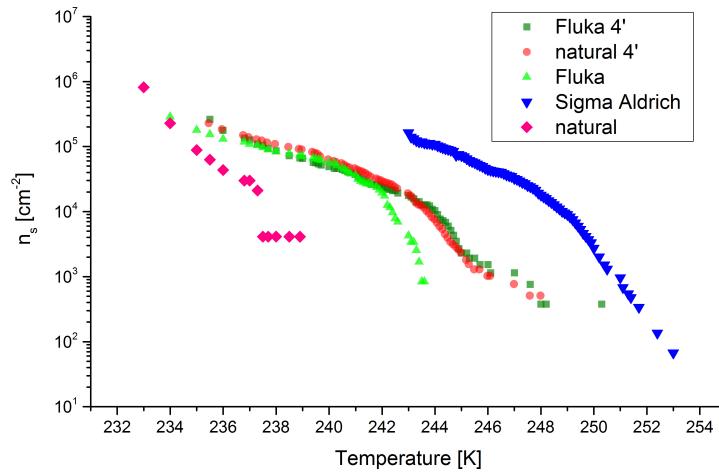


Figure 5.2: Singular model fitting of the quartz samples. The used surface area values were calculated assuming an average drop size of $30\mu\text{m}$ and using the BET surface area values. The active site density was calculated using equation (1.4) in section 1.2.2. The milling of the less active quartz samples shifted the curves to higher temperatures. There is no linear fit between the unmilled and milled natural sample possible, meaning the shift is induced by additional created defects.

further. The enzymes may have different affinities to the sites. Obviously, Papain does not block the very best sites. It may bind to other parts on the particle surface or do not interact with the particles at all. In addition, the concentration of papain is too low to cover the whole available particle surface. The other enzymes block most of these very best sites as only 15% of the spiked droplets freeze above 249K . It was not tested if more enzyme would decrease the ice nucleation further, so it is not possible to determine if the enzymes do only block these very best sites specifically and not the less active ones or if there is not enough enzyme to block all sites. Estimations of the particle and enzyme area show that not enough enzyme, to cover the whole particle surface, was added. The total active site density per drop is still higher in the enzyme treated Sigma Aldrich[®] quartz than in the other two samples even if some sites are blocked. There is still little known about the exact nature of these sites. Klier et al. reported an adsorption of water through surface OH groups of the silica [22]. These hydrophilic sites bind the water molecules, which is in agreement with later studies by Hu et al. on kaolinite [19]. They further report that surface structure, size matching between the ice structure and the solid surface have a strong influence on ice nucleation activity. The above mentioned different samples may vary in these parameters. The coarse quartz sample was almost inactive so the good IN sites are not very common on the crystalline surface. The perfect surface of quartz is thought to not nucleate ice at higher temperature, rather the nucleation takes place at defect sites. Those may be

atomic lattice distortions caused by impurities leading to a better structure matching between the ice and the particle surface or crystallographic dislocations. The immersion freezing results give more than one active site which differ in activity. This could be caused by a different matching between the site and the ice structure or the size of the domain of molecular sites. The worse the matching i.e. the smaller the domain is the lower the nucleation temperature. All the surface defects increase per mass if the surface area is increased, therefore the activity of Sigma Aldrich quartz is higher than the Fluka[®] or the natural quartz and is increased by mechanical milling. In addition, mechanical milling also creates additional defects leading to more or better nucleation sites.

5.1.5 Feldspars

Feldspars are the main building mineral of the silicate rocks on the earth crust and are quite abundant in the atmosphere. The feldspars belong to the tectosilicate group. They have the principal structure of quartz where silicon atoms are replaced by aluminum atoms. The charge difference is compensated by cations. The feldspars therefore have a chemical composition of $Ca_x(Na, K)_{1-x}Al_{1+x}Si_{3-x}O_8$. Natural feldspars have potassium, sodium or calcium as cations to compensate the charge. Impurities of other elements are common, but only in small amounts. The three main phases are K-feldspar ($KAlSi_3O_8$), (high) albite ($NaAlSi_3O_8$) and anorthite ($CaAl_2Si_2O_8$). As represented in the phase diagram a large variety of natural feldspars is known. The different minerals

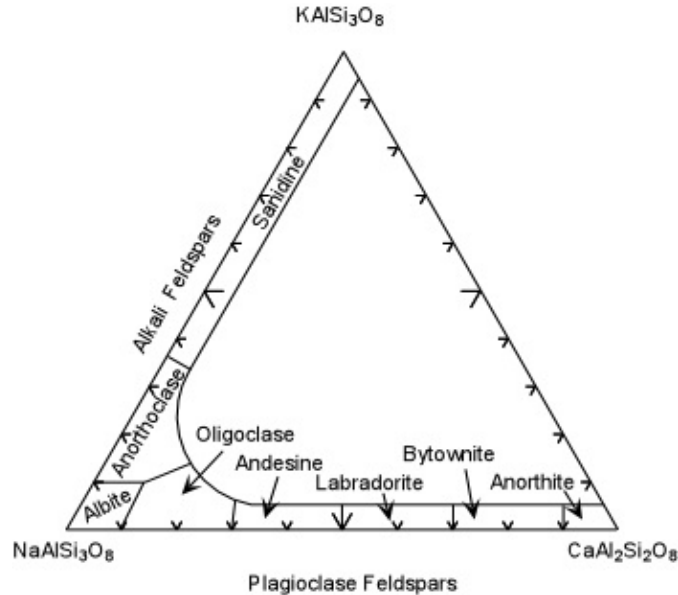


Figure 5.3: Nomenclature of plagioclase feldspar series and high temperature alkali feldspars after Deer, Howie, Sussmann, 1963, rock forming minerals [8]. The alkali feldspars do only form the sanidine phase at higher temperature. Otherwise albite and K-feldspar lamellae form.

do not form solid solutions at all temperatures and lead to even more complex microstructures in nature.

In the feldspars the aluminum atoms replace silicon in a quartz structure. The substitution may be quite regular or more random. Sodium and calcium feldspars are in general more ordered than the potassium analog. K-feldspar occurs in two different phases: microcline and orthoclase. While in orthoclase the aluminum distribution in the crystal is almost completely random, microcline is over 90% ordered. Still the ordering is less than in low-albite. Latest studies by Yakobi-Hancock et al. showed also good ice nucleation activities in the deposition mode for the less ordered orthoclase K-feldspar phase [54]. This leads to the assumption that the increased activity of K-feldspar is not phase specific. Furthermore, the ionic radii of the different cations are different. The ionic radius is hard to define and calculate for solids. The values in literature vary and depend on how the ionic radius is defined. Independent of the used table of ionic radii relation (5.1) is obtained.

$$r_{K^+} > r_{Na^+} \approx r_{Ca^{2+}} \quad (5.1)$$

As a result the unit cell of the K-feldspar is larger than the others' [41]. The SiO_4^{4-}/AlO_4^{4-} tetrahedra in feldspar are slightly tilted due to the charge compensating cations. Surface distortions from the basic quartz structure may even be larger and defects in particular ionic defects are much more common than in quartz. For the immersion freezing experiments on feldspars three different substances were used. As K-feldspar a microcline was used. The powder XRD analysis revealed around 15% sodium-feldspar content on the alkali site. With some EDX mapping albite grains could be identified within the sample. The albite sample had only a very small potassium and calcium content. The SEM-EDX revealed a yield of under <0.5% of the two elements. An anorthian andesine was used as third feldspar sample. XRD revealed a clean sample with a composition of approximately $Na_{0.5}Ca_{0.5}Al_{1.5}Si_{2.5}O_8$.

The immersion freezing experiments were carried out on the hand milled particles. Microcline was the only investigated feldspar active above 243K with a median freezing temperature 249K, while the andesine and albite samples had median freezing temperatures of $240 \pm 1/239 \pm 1$ (fig. 4.1). All these minerals are tectosilicates and have a triclinic structure. The difference in the nucleation temperature between the closely related minerals was thought to be extrinsic or due to impurities in the first explanation. Therefore albite and microcline were treated with different enzymes. The enzymes are able to destroy sugars, proteins and fats. As it is known that biological material is able to nucleate ice the microcline sample might have been active due to these materials (compare Pummer et al. [43]). The enzymes did change the freezing behavior of the microcline sample. The different freezing curves are shown in figure 5.4.

Except for the cellulase onozuka (light blue in figure 5.4) the freezing curves changed drastically by the enzymatic treatment of microcline (red,green). The median freezing temperature shifted to lower temperatures. Further experiments revealed that the loss of ice nucleation activity is a result of an active site blocking and no destruction. Therefore the enzyme treated particles had been heated at 773K for 4h (see section 2.3).

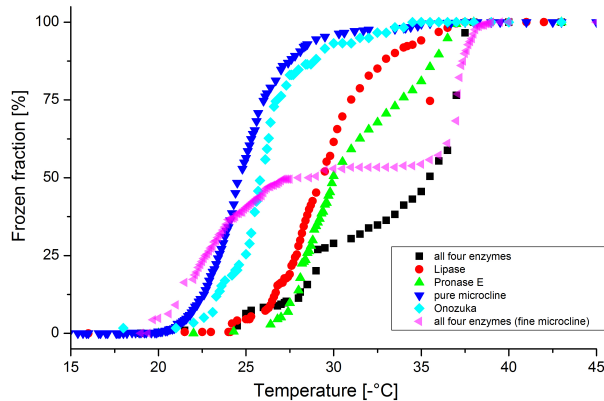


Figure 5.4: Freezing curves of the enzyme treated microcline sample. The microcline particles were treated with only lipase, pronase E, onozuka and all enzymes together with papain. The enzyme cocktail was also applied to the fine milled microcline

The freezing curves after heating were the same as before the enzymatic treatment. In addition the enzymes were mixed with the particles in water. The suspension was put on ice to avoid an enzymatic reaction until the ice nucleation experiment was carried out. The freezing curve looked almost the same as with a normal enzymatic treatment, just the amount of drops freezing heterogeneously was a bit lower. The reason is that the peptidases, which are present in the enzymatic cocktail, partly digest the other enzymes and therefore in the normal enzymatic cocktail less enzymes remain to cover the particle surface. The blocking of the active sites on the microcline surface is not a site specific process, rather the enzymes cover the particles. However, the concentration of the enzymes is too low to cover the whole surface of the feldspar particles. The less frequent very best sites of microcline are covered, but more frequent sites are still uncovered leading to a shift in the freezing curves to lower temperatures, rather than a total loss of the ice nucleation activity of the sample. It is thought that the enzymes only block active sites on the surface and do not destroy any functionality permanently on the particle. If the enzymes are removed by heat treatment the particles are as active as before any treatment. Furthermore adsorbed biological or organic material is destroyed at higher temperatures. Heat treatment of the samples at 373, 523, 773K did not change the ice nucleation property of the microcline sample. In the FTIR spectrum, also no $C - H$ modes were present. If the surface area of the K-feldspar is increased by milling a two step freezing was obtained after enzymatic treatment (pink curve in 5.4). As the enzyme concentration was constant and increased active site density per droplet is assumed based on the decreased particle size, only part of the sites are blocked by the enzymes. The drops containing uncovered active sites freeze like the untreated sample, while the others freeze at lower temperatures by ice nucleation on other sites or homogeneous freezing. The conclusion is that the ice activity of the K-feldspar sample

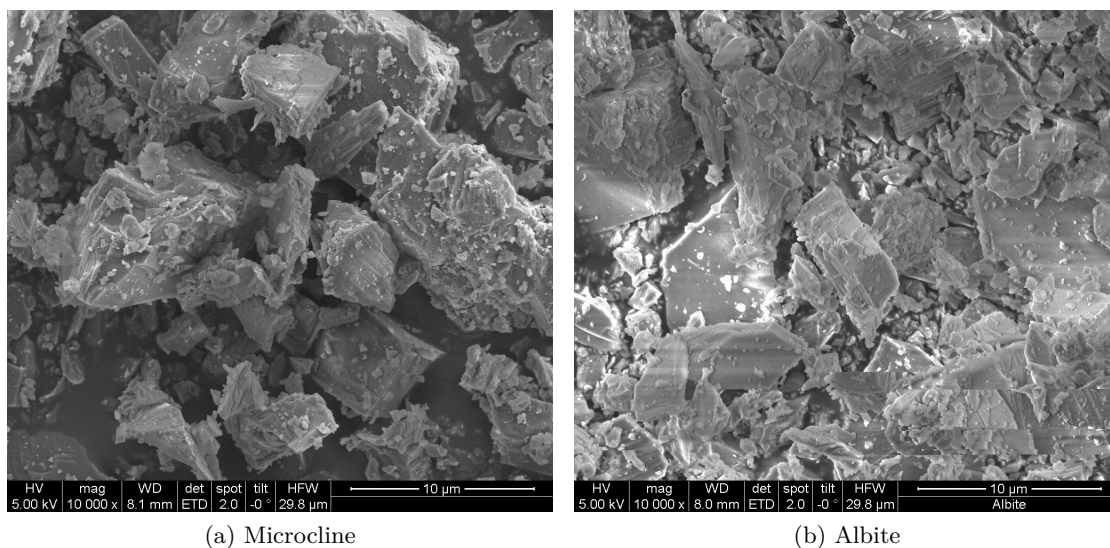


Figure 5.5: SEM images of microcline and albite with a 10.000x magnification.

is an intrinsic property. Nevertheless, the SEM images of the feldspar samples (fig. 5.5) are quite similar and a morphological difference cannot act as an explanation for the different ice nucleation behavior.

Möhler et al. reported that organics are able to suppress ice nucleation on dust particles [32]. To exclude this effect on our albite sample the same treatment as for K-feldspar was applied. The ice nucleation activity did not change after heating and no signature of organic molecules could be seen in the FTIR (see fig. 4.13). In addition the albite sample showed almost no change on the freezing behavior upon enzymatic treatment. The same accounts for the andesine sample, except that enzymatic treatment was not performed on that sample.

Albite and microcline were further studied with TEM (fig.: 4.10,4.14,5.6). The surface structure of microcline is rougher than albite's, but no significant difference in the morphology of the samples could be identified. The albite sample is crystalline and contains nano-sized lead impurities (compare figure 4.14. These impurities appear on some albite grains, while over 70% is highly pure albite. EDX mapping over cracks did not reveal any migration of particular atoms to these sites. If ice nucleation occurs at macroscopic defect sites like cracks it is not due to a local element accumulation.

The microcline sample is almost clean, except the above mentioned albite content. No impurities which may act as IN were found. The sample is crystalline. The atomic composition within the sample does not vary. Impurities or defects are not responsible for the ice nucleation activity difference of the feldspars based on this data, but further studies of more grains are necessary to get a better statistics.

Potassium and sodium belong both to the alkali metal group. The chemical difference is small concerning their electronic properties. Nevertheless, it is known that the surface

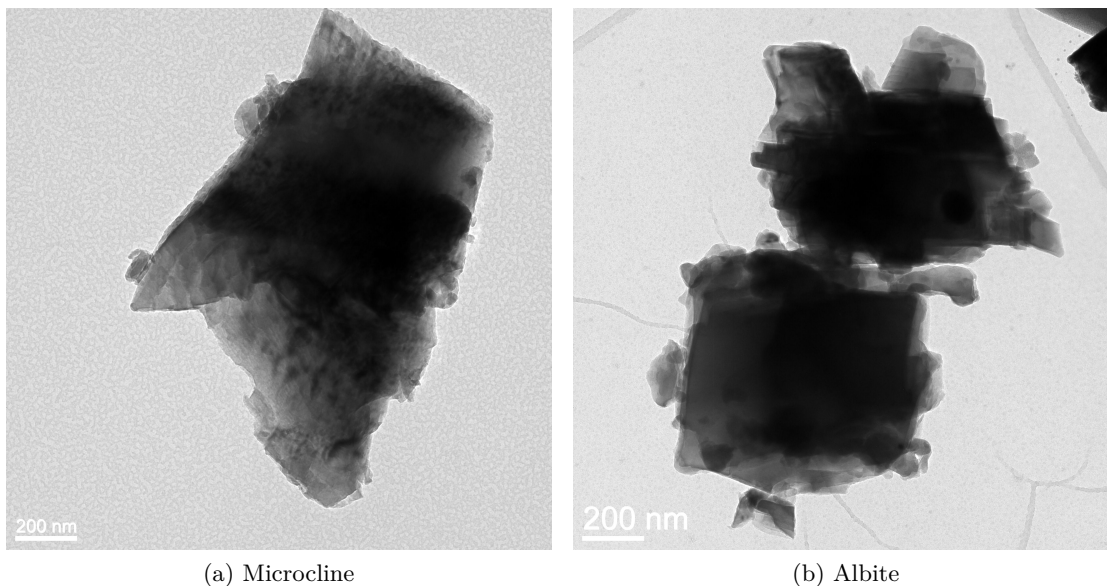


Figure 5.6: TEM images of microcline and albite

of feldspars is depleted partly on the alkali metals in water (compare Fenter et al. [10]). The effect is for example used to separate the feldspars technologically [13]. The exchange of hydrogen, hydronium or water with the cations could play a role in ice nucleation [24]. The exchange rate may be different for the two alkali metals due to the difference in the ionic radii (eq.: 5.1).

The above mentioned measurements leave only the conclusion that the difference in the ice nucleation activity of the feldspars is a result of the difference in the ionic radius of the cations and therefore the local chemical configuration at the surface. Either the surface atoms are at different distances which act as a good template for ice or the surface cations which are released into the surface bilayer may interact with the water to enhance/inhibit ice formation. It was reported that a good matching of the mineral surface and the ice structure is favorable, if not necessary to form a good IN [9,45]. The different sizes of the cations in the feldspar influence the unit cell size and the surface structure. Potassium feldspar has the largest unit cell of the feldspars. The effect on surface distortion may even be larger. The total volume of microcline is around 7% larger than albite. The largest difference of a lattice parameter is around 5%. Functional groups which bind the water in ice favorable positions may be more frequent in microcline than in albite. This could simply be a cation size effect or well attributed to the more random cation/aluminium distribution in the potassium feldspars compared to the calcium and sodium ones.

Despite the different surface matching, which could enable hetero-epitaxial growth of ice on the feldspar surface, the cation-water interaction is important. The ions on the surface have different affinity to water molecules and potential bonds are of different

strength. As mentioned above calcium ions are able to bind the water quite tightly to the surface of calcite and might inhibit ice nucleation by fixing the water molecules in miss-matching locations.

Feldspar surfaces have a cation deficiency at the surface in water. The cations are partly released into the surface bilayer [10]. The tendency of the surface to interact with water molecules is increased by this process. This happens in all feldspars independent of the cation, even if it is not equal for all feldspars (compare Fenter et al. [10,49]). The ions are hydrated in the water matrix. The hydration shells of calcium, sodium and potassium have different sizes and shapes. Calcium and sodium belong to the chaotrope family while potassium is a kosmotrope. Chaotropes are small ions with high charge density. These ions have a strong interaction with water and are considered as structure breaking ions. The weaker water-water hydrogen bonds are broken to form the hydration shells. The residence time of the water molecules on chaotrope cations is much longer than for kosmotropes. These strong chaotrope-water interaction inhibits also ice structure formation in the vicinity of the ions. Kosmotropes like potassium on the other hand have a weaker interaction with water than the intermolecular water-water interaction. The kosmotropic ions are named structure making for this reason. They stabilize water structures. The potassium still forms a hydration shell, but the water molecules are bonded weaker and have high exchange rates. Therefore, any thermodynamical phase change of water is kinetically less hindered than with chaotrope ions [29,55]. The cations of the feldspar, which are released into the water, stay close to the surface of the feldspar due to surface charging. The cations are then able to interact with the water molecules close to the surface. In the case of calcium and sodium ice nucleation is inhibited by their chaotropic behavior, while potassium has a positive or at least neutral effect. In addition, KOH is easily incorporated into the ice structure. The size of potassium is around the size of a hydronium ion, while sodium and calcium are far too small to fit well into the ice structure [44,50]

Washing water samples

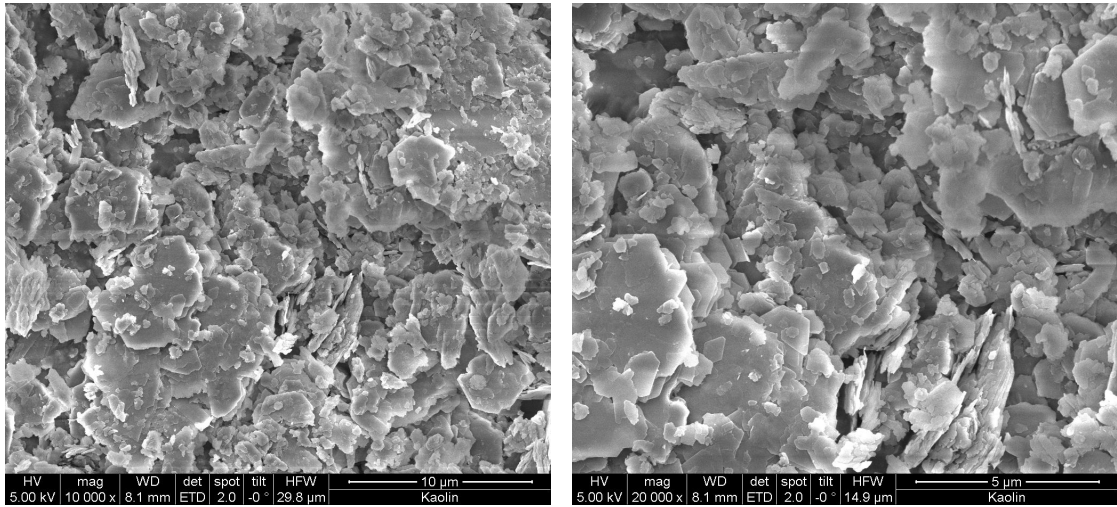
The microcline washing water did freeze partly above homogenous freezing level (see figure 4.12 in section 4.2.2). The same effect was not seen for quartz, albite or andesine. The concentration of particles found in the washing water is very low as a frozen fraction above 90% is not reached before homogeneous freezing. The active component in the washing water of microcline turned out to be microcline particles. Their size was lower than in normal microcline suspensions. The particles which were seen in the SEM were smaller than 500nm. The smaller surface area per droplet than in normal microcline suspensions leads to lower nucleation temperatures due to less active sites per droplet. The concentration of microcline particles is so low that some drops do not contain any particle and freeze homogeneously. The washing water of microcline was the only active washing water of the tested dust samples of quartz, albite and microcline. As the other washing waters were not studied by SEM, it is not possible to mention if particles were present in the washing water of other minerals.

There are two possibilities why the washing water is active for microcline. Either the sedimentation process of the particles in the centrifuge is not perfect and some small particles remain in the solution for all samples. As microcline is the by far most active mineral dust it is still active in such low concentrations while quartz and albite are not. Or the studied microcline sample has some grains that have different sedimentation properties and always stay in the suspension, this can be supported by the fact that a small film was found on top of the used glass tube after centrifugation, which was not found for the other minerals. The active component in the microcline washing water is most likely microcline particles as the activity is lost after filtration with cut-off sizes of 300 and 1000kDA.

5.1.6 Kaolinite

The measured median freezing temperature of the kaolinite sample is $258 \pm 1K$. This value is a lot higher than literature data. The sample contains other minerals than kaolinite. EDX gives 2at% sodium and 1,5at% potassium. This together with the aluminum to silicon ratio gives 15 – 25% of other mineral phases. The XRD gives three other phases which account for 5–10% each. An exact quantification is not possible. The phases are halloysite, quartz and muscovite. At least one of the other mineral phases is a good IN active in the kaolinite sample. Quartz is the first candidate to fulfill this role. Its concentration in the sample is close to 10%. It was shown in the subsection 5.1.4 that quartz has active nucleation sites, but the concentration of those is quite low. In the SEM-EDX measurement no single quartz particle could be identified, so it is difficult to make an estimation of the quartz particle size. There are small particles in the sample, which could be quartz particles (fig. 5.7). Different grains were studied with SEM-EDX. The silicon to aluminum ration was almost the same for all areas in the sample. As all the three other phases have a 1:1 ration, quartz is present everywhere. The quartz could be the small particles seen in figure 5.7. The resolution of the EDX is too low to get the composition of the large particles only, as the small quartz particles are also measured. This leads to the different silicon-aluminium ratio in the EDX-spectrum than the large particle really have.

Those small quartz particles, even if they contribute only to around 10% of the kaolinite sample, have enough surface area to be good IN. Muscovite was seldom studied in the latest years as its concentration in the atmosphere is quite low (fig. 1.9). Muscovite and other micas were found to be able to nucleate ice in the deposition mode, but not better than kaolinite itself [9]. Older studies by Shen et al. found micas to be active IN, but the comparability of these results is questionable [45]. Halloysite concentration is the lowest of the three other phases, but it is commonly mixed with kaolinite in nature. No outstanding difference in ice nucleation behavior between the two minerals had been found [30]. Most likely the active component in our Kaolinite sample is quartz. This is in agreement with the mineral analysis of different kaolinite samples by Atkinson et al. [3]. A kaolinite sample containing K-feldspar is far more active than pure kaolinite. The kaolinite mineral itself is not active above 243K. If active IN are found in the kaolinite matrix like K-feldspar or small quartz particles it is active in immersion freezing



(a) 10.000x magnification of kaolinite

(b) 25.000x magnification of kaolinite

Figure 5.7: SEM images of kaolinite with different magnifications.

experiments. This is in good agreement with Pinti, Murray and Lüönd who found pure kaolinite to be active only below $243K$ [28, 33, 38]. The nucleation process on kaolinite had been proposed as a hetero-epitaxial growth of ice on the surface before. The theoretical kaolinite surface is able to stabilize ice clusters with quite low stabilization energies. The low stabilization energy is a possible explanation for the lower nucleation temperature found for a pure kaolinite mineral. In addition, sodium and other ions are expected to lower the dipolar moment of kaolinite. So there are deviations from the theoretical surface calculated by Hu in natural kaolinite [20].

5.1.7 Montmorillonite

The montmorillonite sample had a low median freezing temperature of $240 \pm 1K$ with initial freezing at much higher temperatures. It is in good agreement with other studies that montmorillonite is not a good IN. An exact quantification of the mineral composition of the sample was not possible. Clean XRD data for montmorillonite is lacking in the data base, an analysis of the different phases is therefore quite difficult. The sample contains many different IN as the freezing curve is quite broad. Good IN are currently represented by 10% freezing above $245K$, but in very low numbers. The rather high initial freezing temperature of the montmorillonite sample is attributed to the other phases present. Quartz and muscovite are found in the montmorillonite sample and both had been found in various studies to be able to nucleate ice. In addition, montmorillonite is a quite soft phyllosilicate with a perfect $2D$ -layered structure. Through mechanical processes, like milling, a stacking fold and gliding of these layers is possible, which may lead to a formation of some nucleation sites.

5.1.8 Natural samples

The volcanic ash sample from Eyjafjallajökull was not a good IN in the immersion freezing mode above $243K$. The initial freezing temperature was around $245K$ which is a result of only very few good IN in the sample. The sample contains mostly albite. This mineral is a bad IN (see section 5.1.5) and therefore the median freezing temperature for the volcanic ash sample is quite low. Most other components like coarse quartz, or calcian-plagioclases are also inactive above $240K$. The active IN is probably K-feldspar.

The shifting of the freezing curves to lower temperatures after milling for a long time is a result of the smaller particle size. The same is well known for ATD [53]. Volcanic ash is neither a good nor a bad IN. Its ice nucleation activity is highly dependent on the mineral composition of the ash. The studied sample did mainly contain the poor IN albite. The K-feldspar content of the sample was rather low and therefore explains the slight activity at higher temperatures. This in turn explains the different ice nucleation results of volcanic ashes mentioned in literature (see chapter 3). The samples were all sampled at different sites or even from different eruptions. The composition of these ashes was not given in the literature, but it varies from eruption to eruption. The three cases mentioned by Hoyle et al. of being a source of good IN, does not nucleate ice at higher temperatures, may even deactivate background IN could be explained that way [18]. In the first case a more active mineral for example K-feldspar was present in higher quantities. The second case is similar as the studied volcanic ash from Eyjafjallajökull with mostly poor IN, like albite, being present in the sample. Finally, volcanic ashes and their by-products formed by sulfuric gases, may deactivate the surface of background IN through coverage with SO_4^{2-} -groups or smaller inactive ash particles.

ATD acts as good IN in the immersion freezing mode. This is no surprise as it contains 15 – 20% of K-feldspar, which is the most active mineral within this study. The other main components are 60 – 65% quartz and 15 – 20% sodium-calcium feldspars. Also quartz has some active sites and may contribute further to the ice nucleation activity of ATD. Nevertheless, in our experimental setup more particles were found in a single drop and only information about the very best site of the particles is obtained. It can well be, that the ice nucleation activity seen on the ATD sample results entirely from the K-feldspar. The ice nucleation activity with a median freezing temperature of $250K$ is in good agreement with literature data [6, 53].

Natural limestone behaved like pure technical calcite in the ice nucleation experiment. Limestone plays no role in atmospheric ice nucleation. More information about the calcite mineral was explained in section 5.1.1.

5.2 Comparison between ice nucleation on different samples and materials

The most active samples nucleated ice around $249K$. Microcline, ATD, Kaolinite, and Sigma Aldrich[®] quartz contain very good nucleation sites. That was the only quartz active at the high temperatures meaning that only few of this very best sites are found on a quartz surface. In comparison the average particle size of microcline was a lot higher. The same activity at a lower surface area means that the surface density of active sites (n_s) in microcline is higher. The feldspars and quartz both are tectosilicates. The basic structure are corner connected SiO_4 tetrahedra, with one third being AlO_4 in the feldspar case. Due to the charge compensating cations in the feldspars the tetrahedra are tilted. This leads to a different morphology of the surface with different atomic distances. For the surface to act as a very good IN a certain set of the surface parameters is necessary. In the K-feldspar this is more common than in quartz leading to many molecular sites forming nucleation sites. The feldspars have more structural perturbations at external surfaces that involve hydroxyl, water and various molecular and ionic defects [47]. In comparison it seems that the very best nucleation sites are quite seldom in quartz. The distortion needed at the surface of quartz may be a result of tiny impurities or crystallographic surface defects and dislocations. These crystallographic defects could be created by mechanical forces, like a particle milling process. The very best sites are not found in the plagioclase family with the same surface area as microcline (K-feldspar). Either the molecular site density is much lower as the cations are smaller in the crystal leading to smaller distortions which do not form a molecular site directly. Or, more likely, sodium and calcium in the feldspar inhibit ice formation by their chaotropic nature (see section 5.1.5). K-feldspar is the only natural tectosilicate which has a high enough n_s -value above $243K$. The potassium ions structure the surface well to form molecular sites and have no negative influence in solution as they can be well incorporated into the ice structure [44, 50]. Further Shen et al. had already suggested the nucleation activity reducing effects of ions with higher charge density [45]. Independent of the site density of the minerals the nucleation temperature is shifted to higher values with increasing surface area per droplet i.e. decreasing particle size. With increased surface area the amount of molecular sites per unit drop-volume in the experiment is increased and larger domains of those lead to sites which are active at higher temperatures. The slight loss of activity after heating can be attributed either to a healing of defects sites meaning a loss of molecular sites or a sintering process reducing the surface area of the sample.

That K-feldspar is the far most active mineral is in good agreement with literature. Atkinson et al. report feldspars for being the best mineral dust particle IN [3]. The data of this work leads to the conclusion that K-feldspar is a far better IN than all other silicates. Both tested plagioclase feldspars (albite and andesine) contain neglectable amounts of K-feldspar for the classical immersion freezing experiment. The Na/Ca-feldspar studied by Atkinson et al. contains around 20% K-feldspar. As they report 4 – 5 particles per investigated droplet, a K-feldspar particle can be expected in almost

every drop leading to ice nucleation at higher temperatures than for pure plagioclase, used in this study. Therefore, they obtained higher median freezing temperatures for their plagioclase sample (Na/Ca-feldspar). The surface area of K-feldspar per droplet in the plagioclase sample was lower in their study as for pure K-feldspar leading to a shift of the median freezing temperature to lower temperatures. The results, presented in this work, are in good agreement with the latest study of Yakobi-Hancock et al. who found plagioclase feldspar within the same range of some clays [54]. Atkinson found quartz to be more active than the clays while Yakobi-Hancock2013 et al. found quartz to be a quite bad IN in the deposition mode. The results presented here for quartz suggest that independent of the studied freezing mode the history of the quartz needs to be considered. Milling experiments revealed that some change in ice nucleation activity can be achieved by creating additional defects by mechanical force on quartz.

The difference in ice nucleation activity of the feldspar group is due to the difference in ionic radius. The results are partly related to Shen et al. who had found lower ice nucleation activities for Al^{3+} doped potassium mica [45]. We expect all feldspars to have quite similar quartz like surface structure as it is known for potassium feldspar that most cations of the surface layer are released into the surface bilayer [10]. The cations in the surface bi-layer interacting with the water molecules increase or decrease the ice nucleating ability of the surface structure.

5.3 Atmospheric impacts of mineral dust particles

Mineral dust particles nucleate ice at temperatures ambient in mixed phase and ice clouds. K-feldspar was the best IN with a comparable surface area. Three other samples were active around the same temperature. K-feldspar particles are common atmospheric aerosols. Feldspar is found in most arid deserts around the world. It seems that a discrimination between the different feldspars is needed in the ice nucleation discussion. Atkinson et al. conclude that K-feldspar is the dominating IN above $248K$ even though K-feldspar does only account for 3% of the atmospheric dust mass. Most clays are weathering products of feldspar, as a result small amounts of the starting material will be found in many natural samples. Since the ice nucleation efficiency of K-feldspar is by far the highest, only small amounts of K-feldspar at the surface are needed for a dust particle to be a good IN as. The nucleation temperature found for immersion freezing can be increased by the suspended particle surface. It is therefore possible that mineral dust particles and in particular K-feldspar are well enough IN to enable further meteorological glaciation processes like the Hallett–Mossop ice multiplication process [3, 54].

Conclusion and outlook

Mineral dust particles play an important role in ice nucleation of mixed phase and ice clouds. The abundance in the atmosphere combined with high freezing temperatures make mineral dust particles good ice nuclei in the atmosphere in the immersion freezing mode. Among the mineral dust particles K-feldspar, in particular microcline, was found to be the most active ice nuclei. K-feldspar is found in many natural dusts and might be the most important dust ice nuclei in the atmosphere. It was further shown in this study that the ice nucleation activity of mineral dust particles could be partly increased by milling of the particles. Mechanical forces are able to create additional defects which enable ice nucleation.

In this thesis a model for heterogeneous ice nucleation on mineral dust particles was presented. The discussed model of a stochastic arrangement of molecular sites could not be verified directly by the experimental data observed. However, the results indicate a closely related mechanism of ice nucleation on mineral dust particles. To further test this hypothesis of ice nucleation more ice nucleation experiments are needed. The observed trend of the increased activity with surface area needs to be separated from the influence of the mechanical milling. Therefore, it would be good to study the ice nucleation behavior of differently concentrated particle suspensions. Increased particle concentrations lead to an increased surface area, available for ice nucleation, per droplet. Furthermore, it is interesting to study the influence of mechanical milling on the particle ice nucleation properties. It is favorable if the surface area of the milled particles is measured.

XPS may be a possible method to study the particle surface in detail. The quartz samples used in this study showed different nucleation behavior which could not only be attributed to the surface area. If impurity atoms are causing the better ice nucleation activity by distorting the perfect quartz surface these could be identified using XPS. It is not easy to study the exact configuration of molecular sites, more sensitive surface methods might reveal the configuration of surface oxygen at the sites.

List of used characters

d	<i>lattice plane distance</i>
Θ	<i>incident beam angle</i>
f_{ice}	<i>fraction of frozen drops</i>
I	<i>electric current</i>
J_{hom}	<i>nucleation rate for homogeneous freezing</i>
J_{het}	<i>nucleation rate for heterogeneous freezing</i>
k	<i>vibrational force constant</i>
λ	<i>wavelength</i>
μ	<i>reduced mass</i>
ν	<i>wavenumber</i>
N	<i>number of drops</i>
Δn_{ice}	<i>frozen drops per time interval</i>
n_s	<i>surface density of active sites</i>
π	<i>Peltier coefficient</i>
Q	<i>heat</i>
r_{ion}	<i>ionic radius</i>
s	<i>surface area</i>
t	<i>time</i>
T	<i>temperature</i>

List of Figures

1.1	Different cloudtypes ©Encyclopedia Britannica, Inc.	2
1.2	Radiation balance of the Earth. Figure taken from Kiehl et al. [21].	4
1.3	The solar spectrum	5
1.4	The structure of water	6
1.5	Phase diagram of water, the figure is taken from University of Bristol web: http://www.enm.bris.ac.uk/teaching/projects/2002_03/jb8355/review.html	7
1.6	The structure of ice I_h	8
1.7	Nucleation modes	10
1.8	Chemical composition of ice-crystal residues, reproduction of data presented by Pratt et al. [40]	12
1.9	The average dust composition from different studies. Data taken from Murray et al. [34]	13
2.1	Scattering model of X-rays, image taken from http://pubs.usgs.gov/of/2001/of01-041/htmldocs/xrpd.htm	18
2.2	The used Bruker Vektor 22 for the FTIR analysis, photo	20
2.3	The used cryo-microscopic setup, photo	23
2.4	Photo of the core of the cryo-cell	24
2.5	Cryo-microscopic images	25
3.1	Computational simulation of an ice layer on a perfect kaolinite surface by Hu et al. [19]	29
4.1	Ice nucleation results of all samples	33
4.2	FTIR spectrum of calcite	34
4.3	SEM images of Calcite	35
4.4	SEM images of gypsum	36
4.5	FTIR and XRD images of gypsum	36
4.6	FTIR spectrum of quartz	37
4.7	SEM images of the different quartz samples	38
4.8	Freezing curves for differently processed quartz samples	39
4.9	SEM image of microcline	40
4.10	TEM images of microcline	41
4.11	Median freezing temperatures for differently treated microcline samples	42

4.12	The freezing curves for the differently treated washing waters of microcline	43
4.13	FTIR spectrum for albite	44
4.14	TEM images of an albite particle with lead impurities	45
4.15	SEM images of andesine	46
4.16	SEM image of Montmorillonite	47
4.17	XRD of montmorillonite	47
4.18	Cryo-microscopic images of the kaolinite sample	48
4.19	SEM image of ATD	49
4.20	XRD of the volcanic ash sample	50
4.21	SEM images of various grains in the volcanic ash sample	51
5.1	Schematic image of active sites on mineral dust particles	54
5.2	singular model fitting of the quartz samples	58
5.3	Nomenclature of plagioclase feldspar series after Deer, Howie, Sussmann, 1963 [8]	59
5.4	Freezing curves of enzyme treated microcline sample	61
5.5	SEM images of microcline and albite	62
5.6	TEM images of microcline and albite	63
5.7	SEM images of kaolinite	66

List of Tables

1.1	The atmospheric gas composition	1
2.1	Mineral samples used in this study	16
2.2	The enzymes used in this study with their corresponding working temperatures	26
4.1	Composition of the microcline sample given by EDX	40
4.2	FTIR peak list for albite	44
4.3	Composition of the montmorillonite given by EDX in the SEM using the K_{α} lines.	47
4.4	Composition of the ATD sample given as oxides in %.	49

Bibliography

- [1] M. Astitha, J. Lelieveld, M. Abdel Kader, A. Pozzer, and A. DeMeij. Parameterization of dust emissions in the global atmospheric chemistry-climate model EMAC : impact of nudging and soil properties. *Atmospheric Chemistry and Physics*, 12:11057–11083, 2012.
- [2] Peter W. Atkins. *Physikalische Chemie*. Wiley-VCH, 3 edition, 2001.
- [3] James D. Atkinson, Benjamin J. Murray, Matthew T. Woodhouse, Thomas F. Whale, Kelly J. Baustian, Kenneth S Carslaw, Steven Dobbie, Daniel O. Sullivan, and Tamsin L. Malkin. The importance of feldspar for ice nucleation by mineral dust in mixed-phase clouds. *Nature*, 498(7454):355–358, 2013.
- [4] Hasan Böke, Sedat Akkurt, Serhan Özdemir, E.Hale Göktürk, and Emine N. Caner Saltik. Quantification of CaCO_3 – $\text{CaSO}_3 \cdot 0.5\text{H}_2\text{O}$ – $\text{CaSO}_4 \cdot 2\text{H}_2\text{O}$ mixtures by FTIR analysis and its ANN model. *Materials Letters*, 58(5):723–726, February 2004.
- [5] Bristol University. <http://www.enm.bris.ac.uk/teaching/projects/>. Accessed: 2013-05-27.
- [6] P. J. Connolly, O. Möhler, P. R. Field, H. Saathoff, R. Burgess, T. Choularton, and Gallagher. Studies of heterogeneous freezing by three different desert dust samples. *Atmospheric Chemistry and Physics*, 9(9):2805–2824, 2009.
- [7] D. J. Cziczo. Single particle measurements of the chemical composition of cirrus ice residue during CRYSTAL-FACE. *Journal of Geophysical Research*, 109(D4):D04201, 2004.
- [8] W.A. Deer, R.A. Howie, and J. Zussman. *Rock-forming Minerals. Volume 4A. Second Edition. Framework silicates: Feldspars*. New York : Wiley, 1962.
- [9] Michael L. Eastwood, Sebastien Cremel, Clemens Gehrke, Eric Girard, and Allan K. Bertram. Ice nucleation on mineral dust particles: Onset conditions, nucleation rates and contact angles. *Journal of Geophysical Research*, 113(D22):D22203, November 2008.

- [10] P. Fenter, H. Teng, P. Geissbühler, J. Hanchar, K. Nagy, and N. Sturchio. Atomic-scale structure of the orthoclase (001)– water interface measured with high-resolution X-ray reflectivity. *Geochimica et Cosmochimica Acta*, 64(21):3663–3673, 2000.
- [11] Gervais, F. and Piriou, B. Temperature dependence of transverse and longitudinal optic modes in α and β phases of quartz. *Physical review B*, 11(10):3944–3950, 1975.
- [12] Hinrich Grothe. *ESF - Workshop - Atmospheric Ice Nucleation: book of abstracts*. Vienna Technical University, 2013.
- [13] I. Gülgönül, C. Karagüzel, and M.S. Çelik. Surface vs. bulk analyses of various feldspars and their significance to flotation. *International Journal of Mineral Processing*, 86(1-4):68–74, March 2008.
- [14] Marvin Haas. The infrared spectrum of gypsum. Technical report, Engineering research institute - University of Michigan, 1955.
- [15] Christoph Hecker, Mark Van der Meijde, and Freek D. van der Meer. Thermal infrared spectroscopy on feldspars — Successes, limitations and their implications for remote sensing. *Earth-Science Reviews*, 103(1-2):60–70, November 2010.
- [16] Thomas E. Hoffer. A LABORATORY INVESTIGATION OF DROPLET FREEZING. *Journal of Meteorology*, 18:766–778, 1961.
- [17] A. Holleman and Nils Wiberg. *Lehrbuch der Anorganischen Chemie*. Walter de Gruyter, 102 edition, 2007.
- [18] C. R. Hoyle, V. Pinti, A. Welti, B. Zobrist, C. Marcolli, B. Luo, Á. Höskuldsson, H. B. Mattsson, O. Stetzer, T. Thorsteinsson, G. Larsen, and T. Peter. Ice nucleation properties of volcanic ash from Eyjafjallajökull. *Atmospheric Chemistry and Physics*, 11(18):9911–9926, September 2011.
- [19] Xiao Liang Hu and Angelos Michaelides. Ice formation on kaolinite: Lattice match or amphoterism? *Surface Science*, 601(23):5378–5381, 2007.
- [20] Xiao Liang Hu and Angelos Michaelides. The kaolinite (001) polar basal plane. *Surface Science*, 604(2):111–117, January 2010.
- [21] J. T. Kiehl and Kevin E. Trenberth. Earth’s Annual Global Mean Energy Budget. *Bulletin of the American Meteorological Society*, 78(2):197–208, February 1997.
- [22] K. Klier, J. H. Shen, and A. C. Zettlemoyer. Water on silica and silicate surfaces. I. Partially hydrophobic silicas. *The Journal of Physical Chemistry*, 77(11):1458–1465, May 1973.
- [23] Daniel A. Knopf and Thomas Koop. Heterogeneous nucleation of ice on surrogates of mineral dust. *Journal of Geophysical Research*, 111(D12):D12201, 2006.

- [24] Andreas K. Kronenberg, Richard Yund, and George; Rossman. Stationary and mobile hydrogen defects in potassium feldspar. *Geochimica et Cosmochimica Acta*, 60(21):4075–4094, 1996.
- [25] Motoi Kumai. Nuclei in Snow and Ice Crystals on the Greenland Ice Cap under Natural and Artificially Stimulated Confitions. *Journal of the Atmospheric Sciences*, 19:474–481, 1962.
- [26] Jennifer S. Lardge, Dorothy M. Duffy, Mike J. Gillan, and Matthew Watkins. Ab Initio Simulations of the Interaction between Water and Defects on the Calcite {1014} Surface. *The Journal of Physical Chemistry*, 114:2664–2668, 2010.
- [27] Jennifer Susan Lardge. *University College London Investigation of the interaction of water with the calcite {1014} surface using ab-initio simulation*. PhD thesis, Univeristy College London, April 2009.
- [28] F. Lüönd, O. Stetzer, A. Welti, and U. Lohmann. Experimental study on the ice nucleation ability of size-selected kaolinite particles in the immersion mode. *Journal of Geophysical Research*, 115(D14):D14201, July 2010.
- [29] Yizhak Marcus. Effect of ions on the structure of water: structure making and breaking. *Chemical reviews*, 109(3):1346–70, March 2009.
- [30] B.J. Mason. The nucleation and growth of ice crystals. *Geophysical Monograph Series*, 1960.
- [31] Werner Massa. *Kristallstrukturbestimmung*. Teubner Studienbücher Chemie, 4. edition, 2005.
- [32] O. Möhler, S. Benz, H. Saathoff, M. Schnaiter, R. Wagner, J. Schneider, S. Walter, V. Ebert, and S. Wagner. The effect of organic coating on the heterogeneous ice nucleation efficiency of mineral dust aerosols. *Environmental Research Letters*, 3(2):025007, April 2008.
- [33] B. J. Murray, S. L. Broadley, T. W. Wilson, J. D. Atkinson, and R. H. Wills. Heterogeneous freezing of water droplets containing kaolinite particles. *Atmospheric Chemistry and Physics*, 11(9):4191–4207, May 2011.
- [34] B. J. Murray, D. O’Sullivan, J. D. Atkinson, and M. E. Webb. Ice nucleation by particles immersed in supercooled cloud droplets. *Chemical Society reviews*, 41(19):6519–54, October 2012.
- [35] D. Niedermeier, R. A. Shaw, S. Hartmann, H. Wex, T. Clauss, J. Voigtländer, and F. Stratmann. Heterogeneous ice nucleation: exploring the transition from stochastic to singular freezing behavior. *Atmospheric Chemistry and Physics*, 11(16):8767–8775, August 2011.

- [36] M Ocana, V Fornes, J V Garcia-ramos, C J Serna, and Instituto De Ciencia De Materiales. Polarization Effects in the Infrared Spectra of -Quartz and -Cristobalite. *Physical Chemical Materials*, 14:527–532, 1987.
- [37] Thomas Peter, Claudia Marcolli, Peter Spichtinger, Thierry Corti, Marcia B Baker, and Thomas Koop. Atmosphere. When dry air is too humid. *Science (New York, N. Y.)*, 314(5804):1399–402, December 2006.
- [38] V. Pinti, C. Marcolli, B. Zobrist, C. R. Hoyle, and T. Peter. Ice nucleation efficiency of clay minerals in the immersion mode. *Atmospheric Chemistry and Physics*, 12(13):5859–5878, July 2012.
- [39] Ulrich Pöschl. Atmosphärische Aerosole: Zusammensetzung, Transformation, Klima- und Gesundheitseffekte. *Angewandte Chemie*, 117(46):7690–7712, November 2005.
- [40] Kerri A. Pratt, Paul J. DeMott, Jeffrey R. French, Zhien Wang, Douglas L. Westphal, Andrew J. Heymsfield, Cynthia H. Twohy, Anthony J. Prenni, and Kimberly a. Prather. In situ detection of biological particles in cloud ice-crystals. *Nature Geoscience*, 2(6):398–401, May 2009.
- [41] Private Author. <http://webmineral.com>. Accessed: 2013-06-01.
- [42] Hans R. Prubbacher and Klett Games D. *Microphysics of Clouds and Precipitation*. Kluwer Academic Publishers, 3. edition, 1997.
- [43] B. G. Pummer, H. Bauer, J. Bernardi, S. Bleicher, and H. Grothe. Suspendable macromolecules are responsible for ice nucleation activity of birch and conifer pollen. *Atmospheric Chemistry and Physics*, 12(5):2541–2550, March 2012.
- [44] Christoph G Salzmann, Paolo G Radaelli, Andreas Hallbrucker, Erwin Mayer, and John L Finney. The preparation and structures of hydrogen ordered phases of ice. *Science (New York, N. Y.)*, 311(5768):1758–61, March 2006.
- [45] J.H Shen, K Klier, and A.C. Zettlemoyer. Ice Nucleation by Micas. *Journal of the Atmospheric Sciences*, 34:957–960, 1977.
- [46] Sigma Aldrich. Sigma aldrich webpage. Accessed: 2013-05-01.
- [47] Josef V Smith. *Feldspars and their Reactions*, chapter Surface Chemistry of Feldspars. Springer, 1994.
- [48] I. Steinke, O. Möhler, A. Kiselev, M. Niemand, H. Saathoff, M. Schnaiter, J. Skrotzki, C. Hoose, and T. Leisner. Ice nucleation properties of fine ash particles from the Eyjafjallajökull eruption in April 2010. *Atmospheric Chemistry and Physics*, 11(24):12945–12958, December 2011.

- [49] S. Lee Swartzen-Allen and Egon Matijevic. Surface and colloid chemistry of clays. *Chemical Reviews*, 74(3):385–400, June 1974.
- [50] Y. Tajima, T. Matsu, and H. Suga. Phase transition in KOH-doped hexagonal ice. *Nature*, 299:810–812, 1982.
- [51] Adrián Villegas-Jiménez, Alfonso Mucci, and Michael A. Whitehead. Theoretical insights into the hydrated (10.4) calcite surface: structure, energetics, and bonding relationships. *Langmuir : the ACS journal of surfaces and colloids*, 25(12):6813–24, June 2009.
- [52] A. Welti, F. Lüönd, Z. A. Kanji, O. Stetzer, and U. Lohmann. Time dependence of immersion freezing. *Atmospheric Chemistry and Physics Discussions*, 12(5):12623–12662, May 2012.
- [53] A. Welti, F. Lüönd, O. Stetzer, and U. Lohmann. Influence of particle size on the ice nucleating ability of mineral dusts. *Atmospheric Chemistry and Physics*, 9:6705–6715, 2009.
- [54] J. D. Yakobi-Hancock, L. a. Ladino, and J. P. D. Abbatt. Feldspar minerals as efficient deposition ice nuclei. *Atmospheric Chemistry and Physics Discussions*, 13(6):17299–17326, June 2013.
- [55] Ronen Zangi. Can salting-in/salting-out ions be classified as chaotropes/kosmotropes? *The journal of physical chemistry. B*, 114(1):643–50, January 2010.
- [56] Frank Zimmermann, Stephan Weinbruch, Lothar Schütz, Heiko Hofmann, Martin Ebert, Konrad Kandler, and Annette Worringer. Ice nucleation properties of the most abundant mineral dust phases. *Journal of Geophysical Research*, 113(D23):D23204, December 2008.